DOE/ER/60773--2

DE91 002760

Technical Progress Report

FUNDAMENTAL QUANTITATIVE ANALYSIS OF MICROBIAL ACTIVITY IN AQUIFER BIORECLAMATION

Bruce E. Rittmann and Albert J. Valocchi
Co-Principal Investigators
Department of Civil Engineering
University of Illinois at Urbana-Champaign

Philippe Baveye
Subcontract Principal Investigator
Department of Agronomy
Cornell University

Sponsored by the
U.S. Department of Energy
Office of Energy Research
Ecological Research Division

Report on Progress from March 1990
through October 1990

1. BACKGROUND

This grant was awarded officially by DOE in March 1989 and renewed for a second year in March 1990. The primary awardee is the Department of Civil Engineering at the University of Illinois at Urbana-Champaign; a subcontract is to the Department of Agronomy at Cornell University. The principal investigators at the University of Illinois are Bruce E. Rittmann and Albert J. Valocchi. The principal investigator at Cornell University is Philippe Baveye.

The University of Illinois also has a closely coupled subcontract, entitled "Modeling the Transport of Biologically and Chemically Reactive Solutes in a Two-Dimensional, Heterogeneous Intermediate Scale Experimental System", from Battelle Pacific Northwest Laboratory (PNL). Progress of the DOE and PNL projects is reported herein.

The project's reporting structure contains two types of reports. The first type is a quarterly internal progress report. The purpose of the internal reports is to keep all members of the research team abreast with developments in each area. The second type is a semi-annual report that is transmitted to DOE and PNL. Its main purpose is to inform the project sponsors of the research-team's progress and plans. This report is the semi-annual progress report for the first half of the second year.

The project has four primary areas: (1) biodegradation of poorly soluble organic contaminants, (2) dual-limitation kinetics of electron donors and acceptors, (3) two-dimensional modeling of biofilm reactions in nonhomogeneous porous media, and (4) biologically induced clogging in porous media. For each area, the following sections give a brief summary of the first year's progress, report this quarter's progress in detail, and indicate plans for future work.

2. BIODEGRADATION OF POORLY SOLUBLE CONTAMINANTS

The key goal of this portion of the project is to investigate fundamental mechanisms controlling in situ biodegradation of nonaqueous-phase liquids (NAPLs) in porous media. The P.I. is B.E. Rittmann, and the research assistant is Eric Seagren.

Previous Accomplishments

During the first year, two compounds were selected for initial experimentation. They are toluene, which represents a NAPL with relatively high water solubility (515 mg/ℓ), and decane, which has very low water solubility (0.05 mg/ℓ). Two potentially useful strains of Pseudomonas putida were obtained. One strain (PpG6) contains the OCT plasmid and aerobically biodegrades decane. The second strain (PpG9) contains the TOL plasmid and aerobically biodegrades toluene.

Critical evaluation of previous fermenter studies on the biodegradation of low-solubility hydrocarbons led to the conclusions that the microbial uptake of very low solubility hydrocarbons probably occurs via direct contact of the bacteria with the hydrocarbon, but the uptake path for high solubility hydrocarbons is from hydrocarbons dissolved in the water.

Experiments utilizing P. putida PpG6 were initiated to evaluate the mass transfer pathways for decane. Batch growth experiments in the presence of liquid decane were carried out. Initially and for the first 12 hours, more cell mass was associated with the decane phase than with the water phase. After 12 hours, the specific growth rate was somewhat higher in the aqueous phase (0.2 versus 0.15/day). These results demonstrate clearly that PpG6 attaches strongly to the decane surface and is not inhibited by decane. The data also suggest that PpG6 can grow on dissolved decane, but they are not conclusive, because the increase in aqueous-phase cells could come from detachment of attached cells.

The Bacterial Adhesion to Hydrocarbons (BATH) test (Rosenberg et al., 1980) was performed with PpG6 to elucidate further its attachment to liquid decane. PpG6 showed little tendency to absorb to decane when grown on nutrient broth, in either the logarithmic phase or the stationary phase; however, PpG6 cells grown on decane showed greater adherence, with the logarithmic phase cells showing the greatest adherence.

Tests with P. putida, PpG9 and toluene as a growth substrate showed that toluene was toxic to PpG9 when liquid toluene was in direct contact with the water. However, PpG9 grew well on toluene when dissolved toluene was diffused into the reaction chamber. Thus, PpG9 will not grow directly on the toluene surface or in locations that have dissolved toluene concentrations near to its solubility limit.

A mathematical model for the simultaneous advection, diffusion, and biodegradation of soluble hydrocarbons was developed for porous media. For the case of steady-state diffusion of NAPL into a semi-infinite pool that is moving with velocity v_x, an analytical solution was derived. This model allows prediction of the concentration of decane or toluene in a two-dimensional grid when no biodegradation is occurring. This model is useful for initial design of an experimental system to evaluate NAPL dissolution into a porous medium.

Progress

A major effort was placed on designing reactors suitable for modeling the in-situ biodegradation of NAPLs. To ensure a good design, the two-dimensional numerical model described in section 4 of this report was modified in order to be able to handle the case in which a NAPL pool is present at the top or bottom of a porous medium. This model was used to evaluate different reactor configurations to be used for laboratory experiments on NAPL dissolution, transport, and biodegradation. In addition, experiments were performed with the

selected organism/compound combinations in order to elucidate the growth kinetics.

Base Designs

In their study of hydrodynamic dispersion, Klotz and Moser (1974) made comparative measurements on quartz sand (0.5 to 1.5 mm) in cylindrical columns of varying diameter and found that, in order to be able to neglect boundary disturbances, the relation between the average grain diameter, d_{50} (i.e., the grain diameter giving 50% by weight passage through the sieve of size d_{50}) and the column diameter, ϕ, must be:

$$\phi \geq 25 d_{50}$$

Using this as a starting point, three initial potential vertical reactor widths -- L_y = 2.5, 5.0, and 7.5 cm — were selected, corresponding to glass bead diameters of 1, 2, and 3 mm, respectively. In the rest of this section, these combinations of reactor widths and bead sizes will be referred to as reactor configurations #1, #2, and #3. The reactor cross section was assumed to be square, with L_z=L_y. Initially, a reactor length, L_x, to vertical width, L_y, ratio of 8 was used, giving reactor lengths of 20 cm, 40 cm, and 60 cm, respectively.

The placement of the NAPL pool in the base designs also had to be established. Again, a guideline was found in the results of Klotz and Moser (1974), who, in their study of hydrodynamic dispersion, made measurements with columns of different diameters, ϕ, and varying distance, L, between the inlet distributor and the first measuring point. They found that in order to obtain reproducible tracer passage curves, it was necessary to fulfill the relationship:

$$L \geq 2 \phi$$

Therefore, in order to avoid problems with entrance effects, the NAPL pools should be placed at least $2L_y$ downstream from the entrance. In addition, the length of the NAPL pool was set at L_y.

Practical Considerations

These basic designs were evaluated in terms of their practicality. The first criterion was the availability of glass beads having the diameters used in the initial sizing of the reactors. While several sources of 3-mm borosilicate glass beads and one source of 2-mm soda lime glass beads were found, no source of 1-mm glass beads was located. Therefore, only reactor configurations #2 and #3 were feasible as initially defined; in further considerations, configuration #1 has 2-mm beads.

Next, the headloss in the three base designs was compared. First, the headloss in clean bed reactors was investigated. The minor headlosses through the inlet and outlet were calculated using the friction factors, K, for sudden enlargement and sudden contraction, as presented by Shames (1982), and the minor headloss equation, $h_L=Kv^2/2g$. The headloss through the porous medium reactors was calculated using the Carmen-Kozeny equation. The 3 reactor configurations were compared using a specific discharge of $q_x=0.1$ m/d; in all three cases, the estimated headlosses were small ($\leq$ 1 mm in all three cases), even with sudden enlargements and contractions at the inlet and outlet (although 91 to 99% of the total headloss was due to the minor headlosses).

Second, the addition of biofilm, its effect on the porosity, and, in turn, the headloss due to clogging in the reactor was investigated. The approach was to assume a range of biofilm thicknesses for the three reactor configurations by assuming a uniform biofilm thickness downstream of L_y-long NAPL pools placed $2L_y$ downstream of the entrance, estimating the porosity with the biofilm present, and calculating the headloss from the NAPL pool to the end of the reactor using the Carmen-Kozeny equation. For all three reactors, three specific discharges — $q_x=0.05$ cm/min, 0.1 cm/min, and 0.2 cm/min — and three biofilm thicknesses — $L_p=0.05$mm, 0.10mm, and 0.20mm — were evaluated. In all three reactor

configurations, the headlosses remain relatively small (< 1 cm) until L_p=0.2mm.

Finally, the three reactor configurations were compared with respect to the feasibility of using a range of specific discharges relevant to the study of groundwater, 0.1 m/d to 10 m/d. The feasibility of the flow rates was evaluated on the basis of pump availability and frequency of feed-solution preparation. Pumps available in our laboratory are suitable for the above range of flow rates for the three reactors. In terms of frequency of making feed solution, the largest aspirator bottle available is 8L. From a practical standpoint, it is necessary to make up 8L of feed solution no more than once every three days. Therefore, the maximum practical flow rate was set at 2.7 L/d. Using this guideline, the practical upper limit for the specific discharges to be used is 4.32 m/d, 1.08 m/d, and 0.48 m/d for reactor configurations #1, #2, and #3, respectively.

Numerical Modeling

The potential reactor configurations outlined above were evaluated using a modification of the two-dimensional model described in section 4. The NAPL pool was treated as first-type boundary conditions with constant concentration equal to the water solubility of the NAPL (515 mg/L for toluene @ 20°C (Verschueren, 1983) and 0.052 mg/L for n-decane @ 25°C (McAuliffe, 1969)). No biodegradation or sorption was included for these configuration-evaluation runs. For all runs of the model, the spatial and temporal grid parameters — Δx, Δy, and Δt — were selected such that the Courant number was less than or equal to 1.0, the Peclet number was less than or equal to 2, the first stability parameter, ρ_1, was greater than or equal to 0.5, and the second stability parameter, ρ_2, was greater than or equal to 0.04 (Frind, 1982).

Several parameters had to be estimated for each solute. The estimates for the diffusion coefficients in water and the effective diffusion coefficients

(i.e., the coefficient of molecular diffusion in the porous medium) for toluene and decane are summarized in Table 2.1.

Table 2.1 Diffusion Coefficients

	Diffusion Coefficient in Free-Solution[1] (cm^2/s)	Effective Diffusion Coefficient[2] (cm^2/s)
Toluene	9.02×10^{-6}	6.04×10^{-6}
n-Decane	6.06×10^{-6}	4.06×10^{-6}

[1]Calculated using the Wilke-Chang equation (Welty, Wicks, and Wilson, 1984).
[2]Calculated using $D_{effective} = D_{free\ solution}\ \tau$, where τ = tortuosity of the granular medium=0.67 (suggested value) (Gillham and Cherry, 1982).

The longitudinal dispersivity, α_L, to be used was estimated using the results of Klotz and Moser (1974) for the longitudinal dispersion coefficient, D_L, as a function of grain size and average linear velocity, $\bar{v}$, of the fluid when dispersion is primarily due to mechanical mixing; therefore, for 2-mm beads, α_L=0.50 cm was used and for 3-mm beads, α_L=1.34 cm was used for $\bar{v}<2 \times 10^{-2}$ cm/s and 0.70 cm was used for $\bar{v}>2$ x 10-^{2} cm/s. These values fall in the range of α_L reported by Gillham and Cherry (1982) as being typical of values of α_L determined in the laboratory (0.01 to 1.0 cm). Values of the transverse dispersivity, α_T, were estimated by assuming that α_L exceeded α_T by a factor of 20; therefore, for 2-mm beads, α_T=0.0250 cm, and for 3-mm beads, α_T=0.0670 cm for $\bar{v}<2 \times 10^{-2}$ cm/s and 0.0350 for $\bar{v}>2$ x 10-^{2} cm/s. For all three reactor configurations, the porosity was assumed to be 0.40, and the background concentration of the dissolved NAPL in the flow system was assumed to be zero.

As a starting point, the three base designs were first evaluated at a specific discharge of 0.1 m/day. The contour plots generated for the three base designs after sufficient time had elapsed to reach a quasi-steady-state are presented in Figure 2.1 for a NAPL pool of toluene. These designs provide the

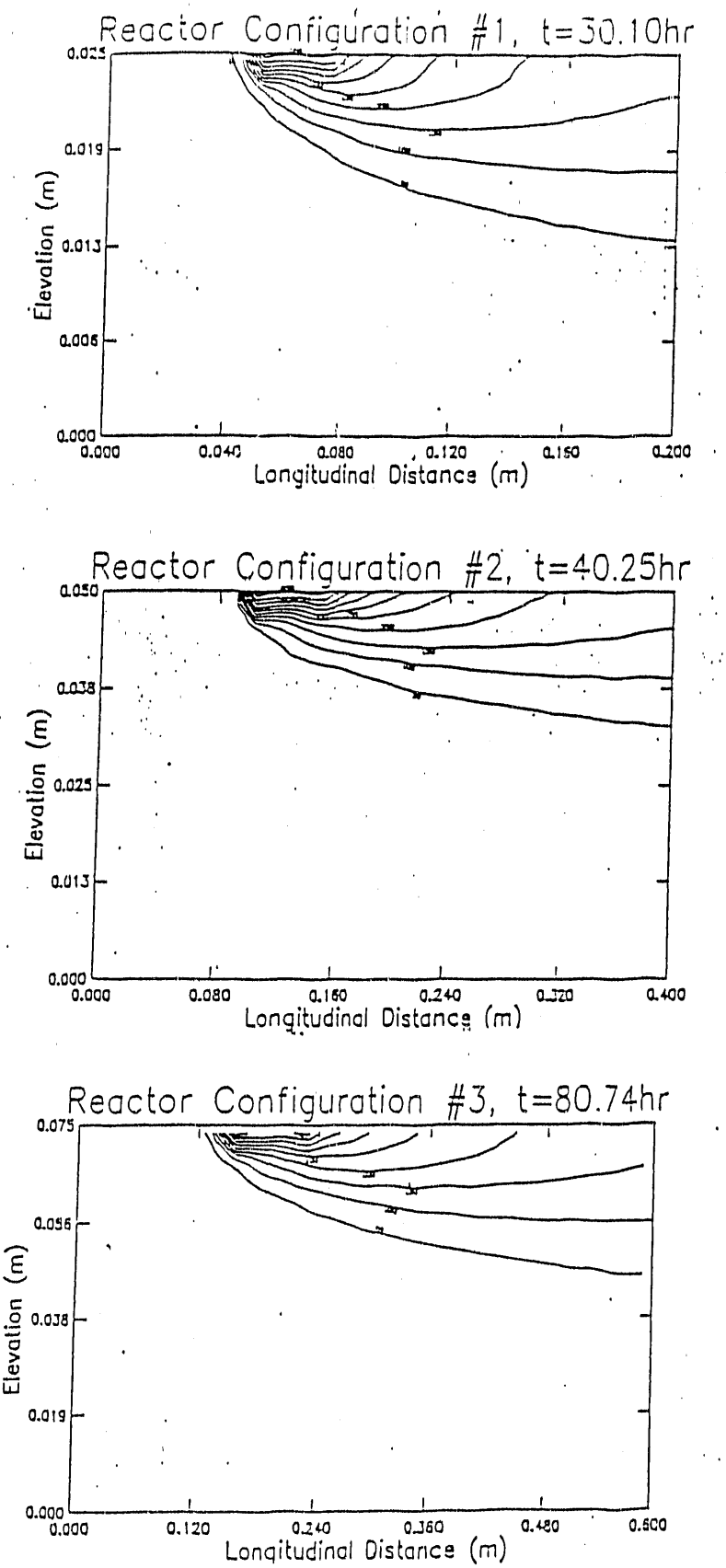

Figure 2.1 Steady-state iso-concentration contours for toluene.

basis for comparison in the following sensitivity analysis.

Sensitivity Analysis

Reactor configurations #1, #2, and #3 were evaluated again at steady state with lengths of 30 cm, 50 cm, and 90 cm, respectively, and contour intervals beginning at 5 mg/L (=0.97% of the water solubility of toluene). Figure 2.2 shows that, for each configuration, the reactor width is adequate to contain a plume with concentrations as low as 5 mg/L. Figure 2.2 also demonstrates that little is gained with respect to plume development by increasing the lengths of the reactor configurations. Indeed, in all three cases, the reactors could actually be made somewhat shorter without significantly changing the nature of the plume; however, the reactor configurations should be kept at least at their current length to allow for the possibility of operating with more than one NAPL pool.

The sensitivity of the reactor designs #1 and #2 to changes in specific discharge was investigated by increasing the specific discharge by an order of magnitude, from q_x=0.1 m/d to 1.0 m/d; reactor configuration #3 was not studied because the frequency of feed preparation is impractical for that design with q_x=1.0 m/d. The contour plots for steady state are presented in Figure 2.3. Comparing these results with those with q_x=0.1 m/d yields two key conclusions. First, as expected, steady state is reached significantly sooner with the higher specific discharge. Second, as the specific discharge is increased, mechanical dispersion increasingly dominates over diffusion, and advection and longitudinal hydrodynamic dispersion dominate over transverse hydrodynamic dispersion. Therefore, the plume does not extend as far vertically downward into the reactor. Analysis of the appropriateness of the width and length of configurations #1 and #2 with q_x=1.0 m/d was performed as before, and it leads to the same conclusions. The reactor width is more than sufficient and, while little is gained by

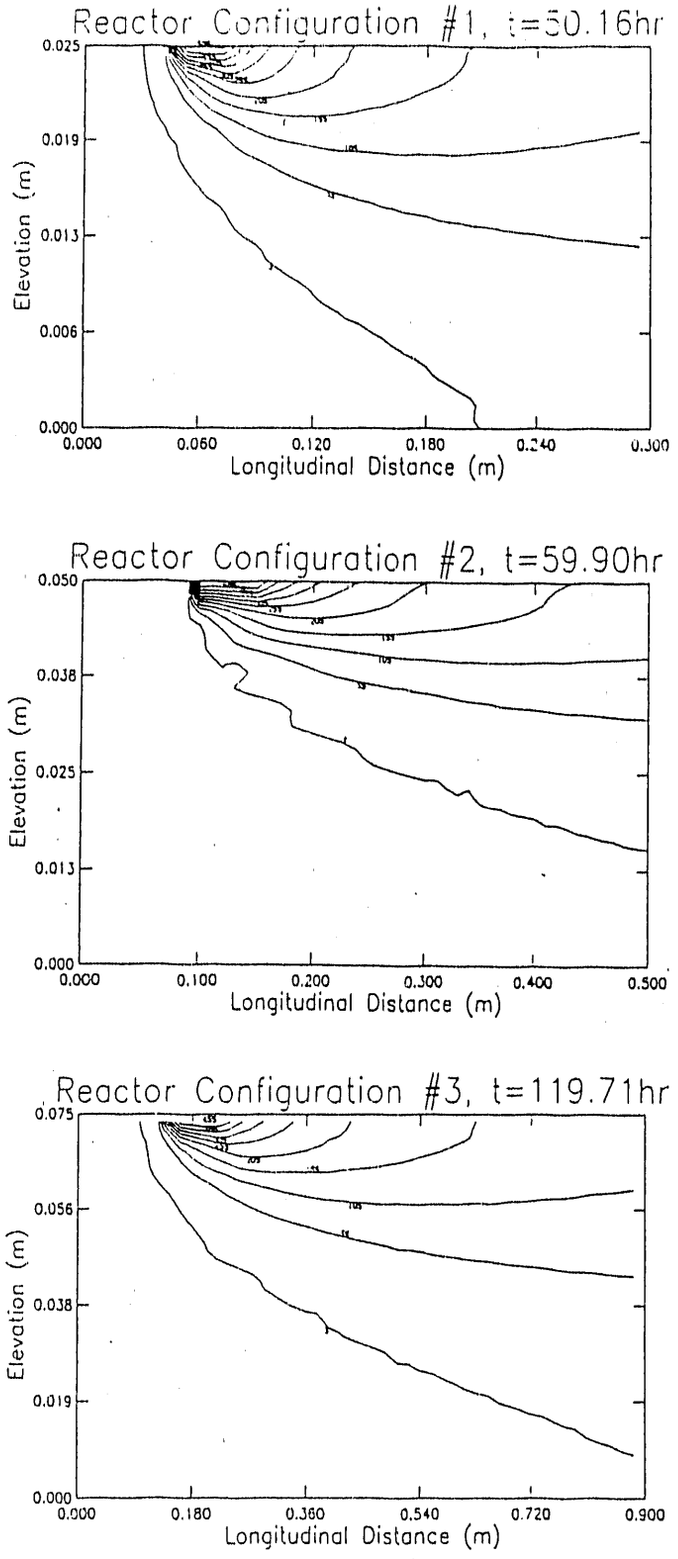

Figure 2.2 Steady-state iso-concentration contours for the base designs, except that the lengths of the columns were increased, compared to Figure 2.1.

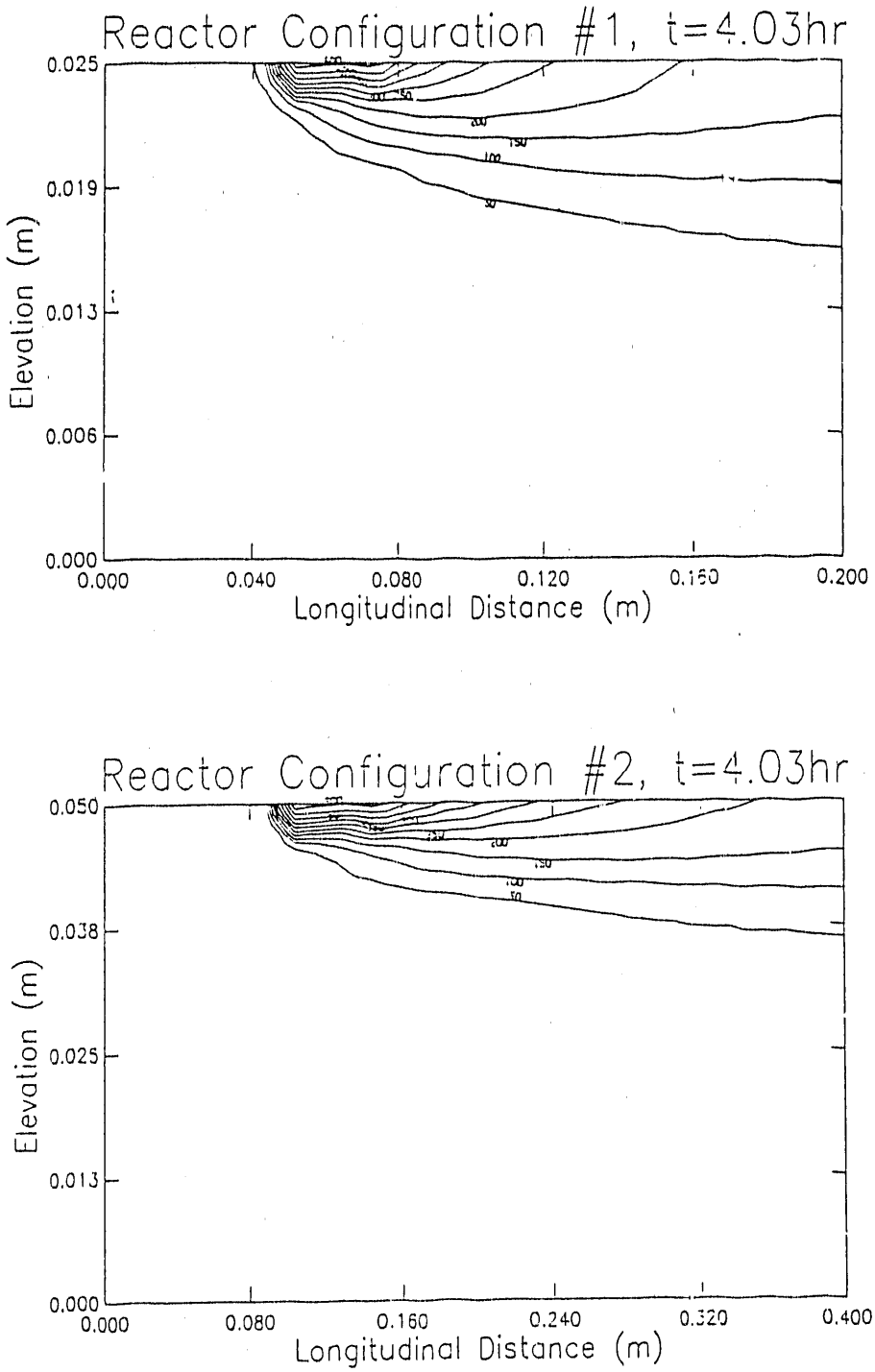

Figure 2.3 Steady-state iso--concentration contours for q_x = 1 m/day.

increasing the reactor length, it probably should not be shortened in order to allow for the use of more than one NAPL pool.

The effect of increasing the longitudinal dispersivity, α_L, and the transverse dispersivity, α_T, by an order of magnitude was also checked. This was accomplished by taking the base design of reactor configuration #2 (2 mm beads, q_x=0.1 m/d) and changing α_L from 0.50 cm to 5.0 cm and α_T from 0.0250 cm to 0.25 cm. This approximated the upper end of the range of values of α_L reported by Gillham and Cherry (1982) as being typical of those found in the laboratory (i.e., 0.01 to 1.0 cm). The contour plot at steady state is shown in Figure 2.4. The time to reach steady state was significantly longer than for the base design. As expected, with the larger longitudinal and transverse dispersivities, the plume spreads to occupy a larger portion of the flow system. The trends for reactor configurations #1 and #3 are similar. Since dispersivities likely will be less than those used to generate Figure 2.4 and the velocities used probably will be greater than or equal to that used in this example, the width of the reactor configurations should be sufficient.

Selection of Reactor Configuration

Based on the analysis of practical considerations and numerical modeling results presented above, all three reactor configurations evaluated have merit, although none is without limitations. Reactor configuration #1 with 2-mm beads is satisfactory in all respects evaluated, except for its ratio of column diameter to bead diameter of 12.5, which is significantly less than the recommendation of 25 by Klotz and Moser (1974). Reactor configuration #2 with 2-mm beads is satisfactory on all accounts, as long as the specific discharge is limited to 1.08 m/d. Similarly, reactor configuration #3 is satisfactory, except that it is even further limited to a feasible specific discharge of 0.48 m/d.

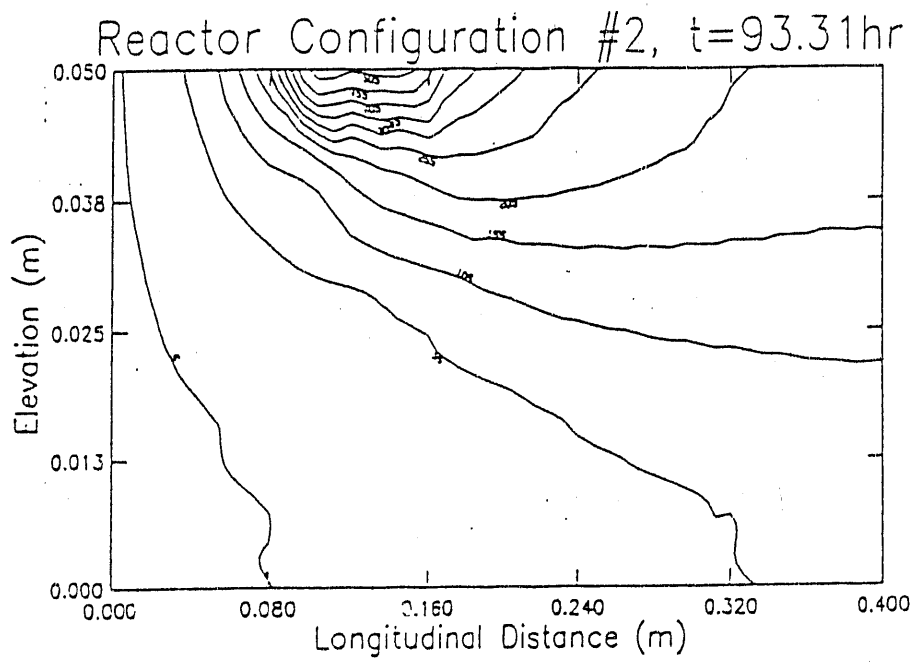

Figure 2.4 Steady-state iso-concentration contours when α_L and α_T are increased 10-fold.

Based on the desire to eliminate boundary disturbances and their effect on plume development, reactor configuration #2 appears to be the best choice at this point. It should be noted that while all of the numerical modeling results up to this point have been shown with toluene as the NAPL, the only real point of difference with n-decane as the NAPL is that the aqueous concentrations of n-decane are significantly lower than those for the toluene plume, due to the lower water solubility of n-decane.

Reactor Construction

The reactor construction needs to satisfy the following requirements: (1) means for containing NAPL pools at various locations and for adding the NAPL to the pool must be provided, (2) ports for sampling various horizontal and vertical locations are required, (3) it must be possible to open up the reactor in order to add or remove the glass beads, and (4) the construction materials for the reactor must be compatible with the NAPLs used.

One possible means for NAPL-pool containment is to place baffles across the width of the reactor on the top wall on 5.0-cm centers (Figure 2.5a). This design, which has eight potential NAPL pool locations, provides good flexibility. In order to minimize interference with the flow caused by the baffles, they should extend no more than two bead diameters (i.e., 4 mm) into the reactor, if possible. A question is how difficult fabrication of a reactor with baffles such as these would be.

An alternative design is to contain the NAPL pool in a space above the reactor wall, such that the NAPL/water interface is flush with reactor wall (Figure 2.5b). This design avoids disturbances in the flow. Borosilicate glass tubing with square cross-section (i.d. = 4.5 and 5.1 cm) is available (Vitro Dynamics), and the glass blower thinks that it can be adapted for this use.

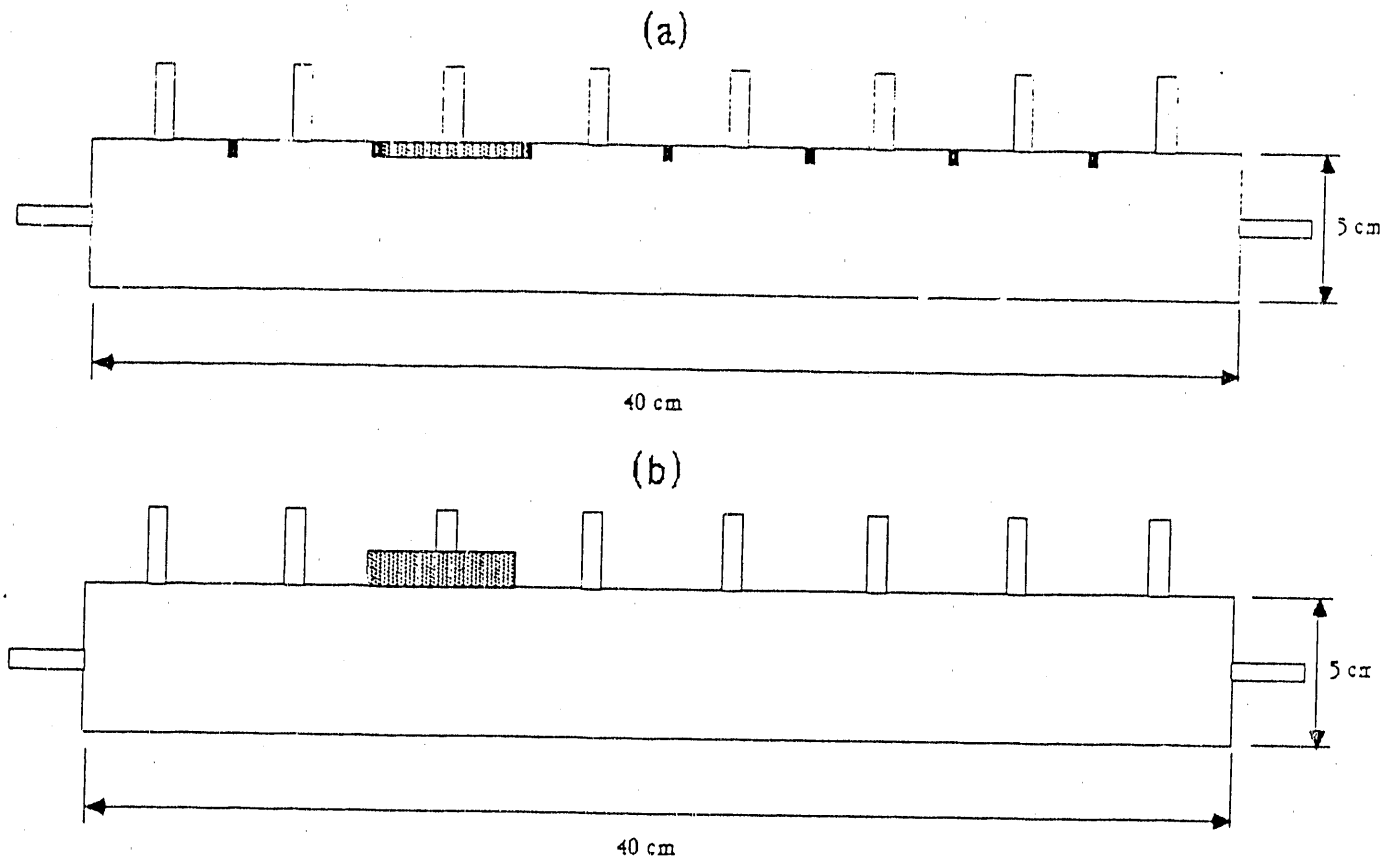

Figure 2.5 Potential means for containment and addition of NAPL pools, side view.

Ports provided along the top of the reactor can also be used for NAPL addition and sampling ports in locations where there is no NAPL pool in place. One possibility is that these ports could be used for sampling at various depths by simply inserting a needle to the appropriate vertical location in the reactor. However, inserting and removing the needles could disturb the dissolved NAPL plume. One possibility is to use the NAPL addition ports for taking samples near the top of the reactor, but provide additional sampling ports placed on the side of the reactor for sampling at vertical locations further from the top of the reactor.

The reactor must be opened to add the glass bead substrata and to be able to remove glass beads for analysis. One possible plan is to make the reactor in three parts: the main body and two endplates with provisions for input and output of flow. To connect the endplates to the reactor body, a slot matching the shape of the walls at the end of the reactor could be cut into the end plate, and a gasket could then be placed in the slot. With these endplates in place, the whole reactor could be held together by inserting four rods, each slightly longer than the reactor and having threaded ends, through holes in each endplate, and then tightening nuts on the end of each rod (Figure 2.6).

The simplest construction material would be plexiglass; however, portions of the reactor are going to be in direct contact with the NAPL, and short exposures of plexiglass to toluene can cause permanent damage. Therefore, the reactor body should be constructed from borosilicate glass. With respect to the endplates, two potential materials are stainless steel and Teflon, of which Teflon would be the easiest to work with in terms of fabrication.

After consultation with the glass blower, we chose a reactor design that has a width and height of 4.5 cm, a length of 36 cm, and contains 2-mm glass beads. The NAPL pool is contained in a reservoir on top of the reactor such that

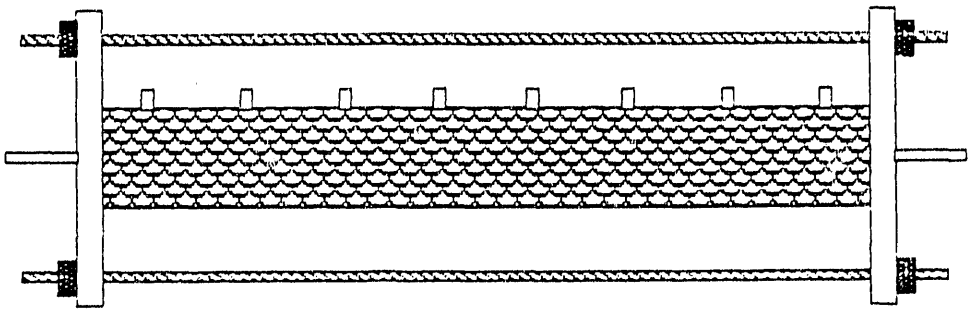

Figure 2.6 Proposed reactor assembly.

the NAPL/water interface will be flush with the top wall of the reactor. Sampling ports are located only along the top wall, because the chances for breakage during fabrication are too great with added ports placed along other walls. Sampling is performed by inserting a needle to different depths. The sample ports are 2-mm ID x 6-mm OD glass tubes that are flush with the inner-wall surface and extend 2.5 cm above the wall. Figure 2.7 gives the reactor design. Fabrication of this reactor is not easy; therefore, some changes may be needed to allow its fabrication.

Organism/Compound Combinations

Prior work showed that decane was a good model for low-solubility alkanes. Unfortunately, the source of C-14-labelled decane is no longer available. Therefore, we shifted the low-solubility compound to dodecane, which is available with a C-14 label.

A search for a dodecane utilizing bacterium was initiated. An excellent candidate was isolated from a reactor in our laboratory. Given the tentative name of isolate DA, the isolate appears to utilize dodecane as a carbon and energy source in liquid and plate cultures. Although additional verification is needed, isolate DA seems to be an excellent candidate for biodegradation of dodecane.

The high solubility compound is toluene, and the microorganism is Pseudomonas putida PpG9. Methods to estimate the kinetic parameter for this substrate/organism combination were begun.

In order to obtain the necessary kinetic coefficients, means for measuring biomass and substrate concentration are needed. A common technique used for measuring biomass concentration is by measuring the absorbance or turbidity, which is converted to biomass concentration using a prepared calibration curve of absorbance versus biomass concentration (Koch, 1981).

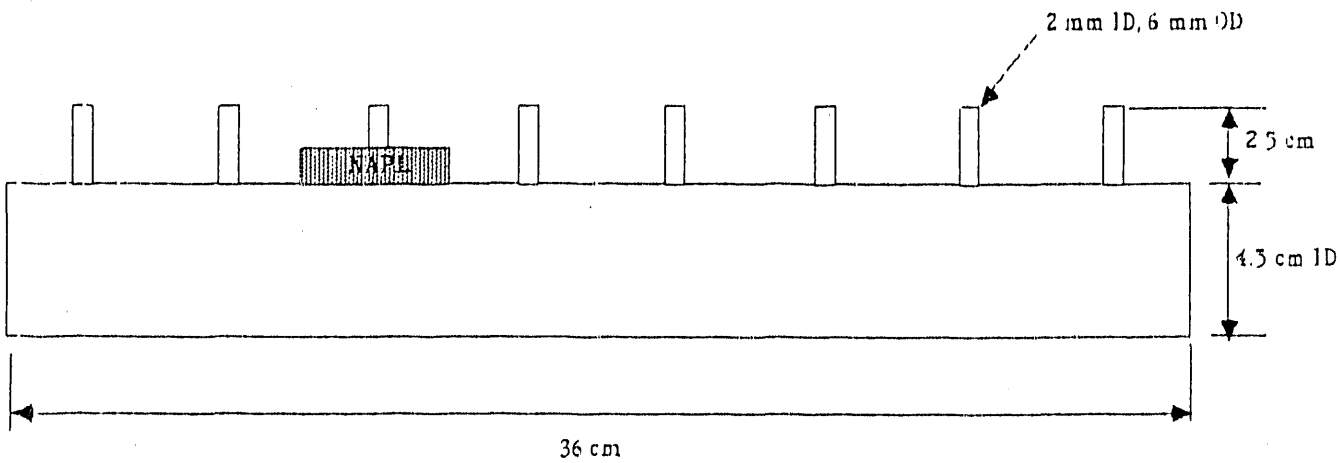

Figure 2.7 Modified Reactor Design.

For measuring toluene concentration, two possible methods are available: ultraviolet (UV) spectrophotometry and gas chromatography. So far only the UV spectrophotometric method has been investigated, and it will be discussed briefly here; this would be a convenient method to use, since the cell turbidity and toluene could be measured rapidly in the spectrophotometer. The first step was to perform a UV scan of absorbance versus wavelength, from which a wavelength suitable for quantitative analysis could be chosen (Fritz and Schenk, 1979). The absorption spectrum of an approximately 250 mg/l toluene in distilled water solution is shown in Figure 2.8a. Here the solvent used was distilled water, but often other solvents such as cyclohexane are used, primarily because of the higher solubility of the compounds of interest (Friedel and Orchin, 1951). An absorption spectrum was also performed after extracting the toluene into hexane, as described by Miller et al. (1990); the locations of the peaks and their magnitude was altered somewhat. However, the use of water as the solvent seems more appropriate, because its use as simple and only concentrations less than or equal to the water solubility limit is relevant. A sample calibration curve of absorbance versus concentration was prepared using 260 nm (similar to the 262 nm used by Miller et al. with toluene extracted into hexane) as the wavelength and water as the solvent. The relationship was linear ($r = 0.96$).

One concern with the UV method is the possibility of interference by other compounds in the culture broth. To begin to address this question, an absorption spectrum was performed with culture broth of cells grown on toluene (Figure 2.8b). Although the toluene peaks are easily identified, the absorbance baseline increases as the wavelength goes from 700 to 200 nm. Three possible explanations exist. First and probably most important is the possibility of interference by chemical intermediates in the toluene degradation pathway encoded by the TOL plasmid. Many of the intermediates have carbon-carbon and/or carbon-oxygen

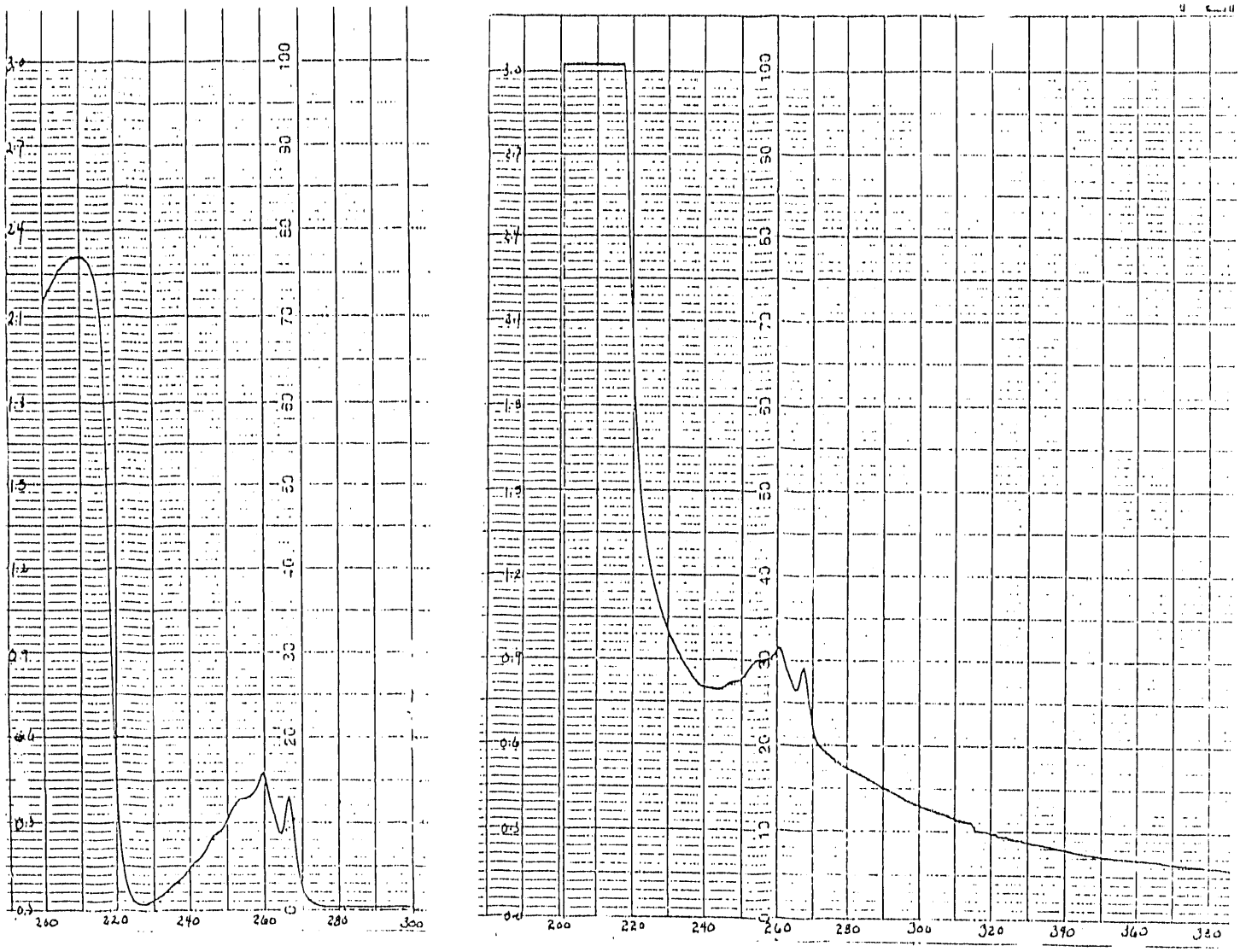

Figure 2.8 Absorption spectra: (a) approximately 250 mg/L toluene in distilled water; (b) culture broth of P. putida PpG9 grown on toluene in mineral medium.

double bonds (Burlage et al., 1989), both of which are chromophores that absorb in the ultraviolet region (Fritz and Schenk, 1979). Second, the culture broth was slightly turbid with cells and had a greenish color. Third, inorganic species with a nonmetal atom doubly bonded to oxygen (examples in the mineral medium being SO_4^{2-} and PO_4^{3-}) absorb in the ultraviolet region (Fritz and Schenk, 1979). Based on Fig. 2.8b, it appears that, while the toluene peaks are easily identified in the culture broth, it is not yet clear whether or not the above mentioned factors interfere with the quantification of the amount of toluene.

One complicating factor in the determination of the growth curves with toluene as the substrate is the volatility of toluene (Henry's constant, K_H = 5.7 x 10^{-3} atm•m^3/mole = 0.18 mole/L•atm). This leads to problems when it comes to providing the oxygen without stripping the toluene. One possible approach is to have no head space in the batch reactors and to provide the oxygen by adding hydrogen peroxide. This approach, however, replaces the problem of volatilization with that of the toxicity of hydrogen peroxide. Some preliminary experiments were performed to begin to elucidate the effect of H_2O_2 on PpG9. As a first step, experiments were performed in which various amounts of H_2O_2 stock solution were added to 13 x 100 mm test tubes of PpG9 cells growing exponentially on nutrient broth such that the cells in different tubes were exposed to H_2O_2 concentrations of 8, 6, 4, 2,, 1, 0.5, 0.1, and 0.05 mM. In all cases with H_2O_2 $\geq$ mM, there was no additional growth (i.e., turbidity increase) after H_2O_2 addition; in fact, the turbidity decreased with time. In all cases for $H_2O_2 \leq$ 1 mM, the turbidity when the experiment was concluded was between 65% and 93% of what would be predicted based on dilution of the control tubes by the volume of H_2O_2 stock solution added. Within the accuracy of the method used, this was taken as an indication that, for dense cultures of exponentially growing PpG9, concentrations of $H_2O_2 \leq$ 1 mM have little or no inhibitory effect on the cells.

On the other hand, addition of 1 mM H_2O_2 to cultures growing slowly due to low substrate availability showed inhibition. These results are similar to those of Pardiesk et al. (1990). The H_2O_2 results with low concentration of substrate illustrate the weakness of using H_2O_2 as an O_2 source. Addition of catalase enzyme to rapidly decompose H_2O_2 may be an alternative for mitigating H_2O_2's inhibition effects on slow-growing cultures.

Future Directions

Once the column reactors are fabricated, abiotic experiments will be carried out first. These tests will be used to evaluate the experimental procedures and to test the two-dimensional model without reaction. Future work on biodegradation will emphasize the evaluation of isolate DA and obtaining kinetic parameters for DA and P. putida PpG9.

3. DUAL-LIMITATION KINETICS

Dual limitation refers to a situation in which the electron donor and electron acceptor limit the cell-growth rate together. The P.I. for this portion of the research is B.E. Rittmann, and the research assistant is Wookeun Bae.

Previous Accomplishments

A literature review revealed that bacteria respond to decreases in electron donor or acceptor by altering their concentrations of internal substrates. Under electron-donor depletion, the NAD/NADH ratio increases (Matin and Gottschal, 1976), while NAD/NADH and ATP/ADP ratios decrease under electron-acceptor depletion (Harrison et al., 1969; Wilson et al., 1977). A structured kinetic model was presented in the first semi-annual progress report. The model expresses the overall rate of substrate utilization as a function of the concentrations of each substrate, stoichiometry, and response factors for NAD/NADH and ATP/ADP.

An experimental program using chemostats was described. The specific growth rate and the concentrations of acetate and O_2 are varied. Two Pseudomonas putida strains, PpF1 and PpG9, were selected for initial experimentation. Because PpF1 gave a higher maximum specific growth rate and a higher true yield coefficient, it was selected for further experimentation.

In the second semi-annual progress report, very sensitive techniques for measuring NAD, NADH, ATP, ADP, and internal inorganic P were described. NAD and NADH are measured by a fluorescence measurement in which fluorescent resorufin is enzymatically produced at a rate proportional to the concentration of NAD or NADH. ATP and ADP are measured by bioluminescence with firefly luciferase. Inorganic orthophosphate is assayed spectrophotometrically after color formation by reaction of phosphomolybdate with malachite green.

Preliminary chemostat experiments were performed with acetate limitation. NADH concentrations rose when the dilution rate (and acetate concentration) increased, but NAD did not change much. Thus, the NAD/NADH ratio decreased as the dilution rate was increased as anticipated. Again as expected, the ATP/ADP ratio remained relatively constant. These experiments confirmed the analytical and experimental methods.

Progress

Six areas of progress were achieved during the past six months. The first four relate to improvements in the experimental methods. The fifth involves a method for data interpretation. The sixth is new experimental results with electron-donor or electron-acceptor limitation.

Experimental Methods

Acetate concentrations are very low under electron-donor limitation and cannot be determined by conventional methods. One aspect of the measurement problem is that the already low acetate concentration is reduced further during

the time required for conventional sample filtration. To overcome this aspect of the problem, an *in situ* filtration method was employed. A membrane filter is inserted directly into the chemostat, and sample is sucked through it, instantaneously removing all cells. The filter is attached to a syringe-type filter assembly that was modified by removal of the filter assembly facing the reactor medium.

The second aspect of the acetate-measurement problem is that the concentration is too low for GC determination without extensive concentration, which is tedious and fraught with opportunities for inaccuracies. A novel bioassay determination scheme was developed to overcome the sensitivity problem. A small inoculum (0.1 mℓ) of cell suspension is taken from the chemostats and is transferred at time = 0 to a batch reactor that already contains 10 mℓ of filtered medium that has in it a small concentration of ^{14}C-acetate. The instantaneous filtration method is used to withdraw samples over time, and the samples are assayed by scintillation counting. The ^{14}C-acetate declines over time, as shown in Figure 3.1. The initial specific utilization rate is determined by the slope of the line as it is extrapolated to time = 0. The initial specific utilization rate ought to be the same as the specific utilization rate in the chemostat, because both systems have the same acetate concentration, S^e. The specific utilization rate in the chemostat is computed from

$$\frac{S^o - S^e}{\theta X_{ch}}$$

in which S^o = influent acetate concentration to the chemostat

θ = detention time of the chemostat

X_{ch} = cell concentration in the chemostat

In the small batch reactor, the initial specific utilization rate is computed as

$$\frac{S^{\circ}}{t^{*}X_b}$$

in which t^{*} = intercept on time axis (see Fig. 3.1)

X_b = cell concentration in the batch reactor

Setting the specific utilization rates equal and solving for S° give

$$S^{\circ} = \frac{S^{\circ}t^{*}X_b}{\theta X_{ch} + t^{*}X_b} \qquad (3.1)$$

Although the previously reported methods to measure NAD and NADH are satisfactory, they were modified to allow for more rapid determination of multiple samples. In the modified method, thiazolyl blue is the added reactant. It forms a blue color that can be measured in a common spectrophotometer (Bernofsky and Swan, 1973). The color reaction for many samples can be carried out simultaneously in a 30°C water batch. Iodoacetate is added to quench the reaction.

A new chemostat reactor was designed to take advantage of the new instantaneous filtration method for sampling, to allow continuous D.O. measurement, to have temperature control, and to avoid contamination of the culture. The new reactor has a 200-mℓ liquid volume. It is completely closed to the environment, except for the feed and effluent lines and sampling ports. It is surrounded by a water jacket for temperature control. Oxygen supply is achieved through feeding of H_2O_2, which is quickly converted to O_2 by catalase.

The new reactor is called the daughter reactor (DR), because it receives its inoculum from a 1-ℓ mother reactor (MR), which is operated continuously as a constant source of P. putida PpF1. The DR is operated as a chemostat. Because the MR is not affected by any events in the DR, the culture at the MR cannot be contaminated.

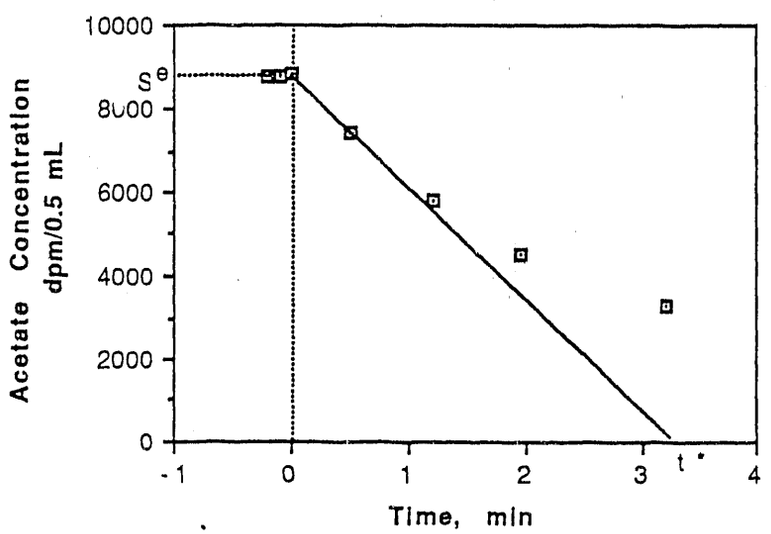

Figure 3.1. Determination of initial reaction rate for <u>in situ</u> filtrate batch test in S1-.087.

Data Analysis

Equation 3.2, taken from the first semi-annual progress report, gives the expected functional variation of the electron-donor specific utilization rate, q_d, with S_a and S_d. Effects of internal substrates already are embedded in the various parameters in Equation 3.2.

$$-q_d = \frac{1.6386\phi q_{ma}' q_{md}' \left(\frac{S_a}{K_a+S_a}\right)\left(\frac{S_d}{K_d+S_d}\right)}{\beta q_{ma}' \left(\frac{S_a}{K_a+S_a}\right) - \nu_{a/d}\beta' q_{md}' \left(\frac{S_d}{K_d+S_d}\right) + 0.0418 Y_d \phi q_{ma}' q_{md}' \left(\frac{S_d}{K_d+S_d}\right)} \tag{3.2}$$

From the first semi-annual progress report, two other equations for the rate of electron-acceptor and electron-donor utilization rates are

$$-r_a = \frac{q_{ma}' \log([NAD/NADH]^{\alpha}[ATP/ADP]^{\beta}) S_a X}{K_a + S_a} \tag{3.3}$$

$$-r_d = \frac{q_{md}' \log([NAD/NADH]^{\alpha'}[ATP/ADP]^{\beta'}) S_d X}{K_d + S_d} \tag{3.4}$$

Four key parameters must be evaluated experimentally: $\alpha q_{ma}'$, $\beta q_{ma}'$, $\alpha' q_{md}'$, and $\beta' q_{md}'$.

When the electron-acceptor concentration is high ($S_a >> K_a$), Equation (3.3) reduces to

$$-r_a/X = q_{ma}' \log([NAD/NADH]^{\alpha}[ATP/ADP]^{\beta}) \tag{3.5}$$

Rearrangement of Equation 3.5 gives

$$\frac{-r_a/X}{\log[ATP/ADP]} = \alpha q_{ma}' \frac{\log[NAD/NADH]}{\log[ATP/ADP]} + \beta q_{ma}' \tag{3.6}$$

Thus, Equation 3.6 shows that $\alpha q_{ma}'$ and $\beta q_{ma}'$ can be found from the slope and intercept of a plot of data for electron-donor limitation. In a similar manner, the terms $\alpha' q_{md}'$ and $\beta' q_{md}'$ can be obtained from data with electron-acceptor limitation,

$$\frac{-r_d/X}{\log[ATP/ADP]} = \alpha' q_{md}' \frac{\log[NAD/NADH]}{\log[ATP/ADP]} + \beta' q_{md}' \qquad (3.7)$$

Experimental Results

Two series of chemostat experiments were completed. In series S1, the electron donor, acetate, was always rate limiting. In series S2, the electron acceptor, O_2, was limiting. For series S1, the DR was operated under electron-donor limitation at T = 27°C, pH = 7.5, and D.O. = 1.8 mg/ℓ. The results for four runs are presented in Table 3.1.

Table 3.1 Steady-State Concentrations of External and Internal Substrates in Short-Term Chemostat Experiments for Series S1.

Run Designation	S1-.029	S1-.087	S1-.174	S1-.385
Dilution rate, hr^{-1}	0.029	0.087	0.174	0.385
Acetate, mg COD/L	>0.010	0.056	0.43	0.87
$-r_a/(-r_d)$, mg DO/mg COD	0.714	0.633	0.586	0.558
NAD, μmole/g cells	4.0	3.6	4.8	4.8
NADH, μmole/g cells	0.063	0.084	0.12	0.22
NAD/NADH	63.2	42.8	40.4	27.5
P_i, μmole/g cells	-	51	60	74

Consistent with the literature and our previous work, increasing dilution rate gave an increasing acetate concentration and a decreasing NAD/NADH ratio. Internal P concentrations (P_i) increased slightly with increasing dilution rate. Unfortunately, ATP and ADP concentrations could not be determined well, and these experiments must be performed again.

Although ATP/ADP ratios were not available, our previous work showed that they were relatively constant. An assumption of a constant ATP/ADP ratio was used to generate Figure 3.2, the slope of which gives $\alpha q_{ma}' = -3.37\ hr^{-1}$. The apparent linearity of the data in Figure 3.2 supports the model. The parameter $\beta q_{ma}'$ can be determined once the values of ATP/ADP are determined.

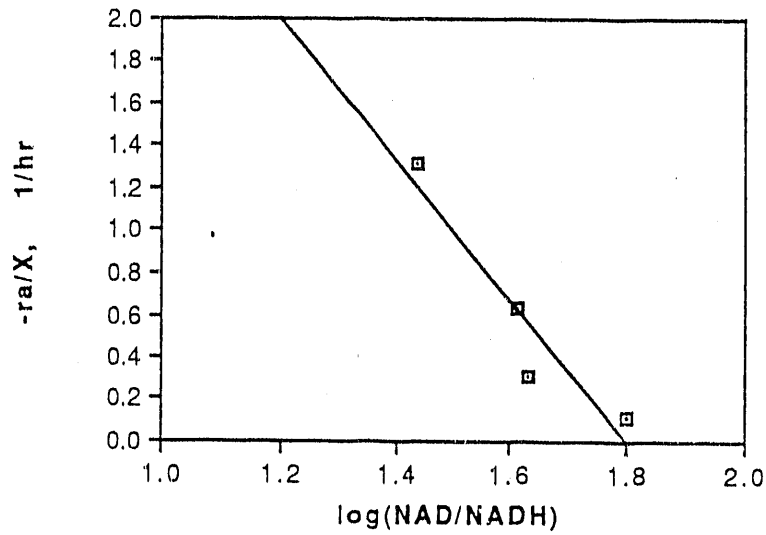

Figure 3.2 Determination of the parameter $\alpha q'_{ma}$.

Series S4 was performed under oxygen limitation by supplying sufficient acetate (c. 1000 mg/ℓ of COD) and controlling the O_2 concentration by the rate of H_2O_2 feeding. Dissolved oxygen (DO) was measured using the sensitive DO meter.

The results for series S4 are summarized in Table 3.2. As the dilution rate was lowered, a lower DO concentration was achieved. The results demonstrate that DO was rate limiting, as expected. NAD, NADH, and the NAD/NADH ratio did not change dramatically as the dilution rate and DO concentrations varied, although NAD and the ratio tended to increase for lower dilution rates (and DO concentrations). What is dramatic is that the NAD/NADH ratios for series S4 (ratios of 1.8-5.6) were much lower than for series S1 (ratios of 27.5-63.2). The lower NAD/NADH ratios present with no electron-donor limitation are consistent with our hypothesis that higher electron-donor concentrations allow a smaller NAD/NADH ratio.

Table 3.2 Steady-state concentrations of external and internal substrates in short-term chemostat experiments under oxygen limitation, Series S4.

Run Designation	S4-.033	S4-.08	S4-.15	S4-.31	S4-.38
Dilution rate, hr^{-1}	0.033	0.08	0.15	0.31	0.38
DO, μg/L	2.0	3.7-7.7	12	27	45-55
NAD, μmole/g cells	4.2	4.1	3.4	3.6	3.7
NADH, μmole/g cells	1.1	0.73	0.89	2.8	1.45
NAD/NADH	3.8	5.6	3.9	1.8	2.6
ATP, μmole/g cells	7.4	7.4	6.1	6.2	6.7
ADP, μmole/g cells	3.3	2.5	3.6	4.4	4.6
ATP/ADP	2.3±0.4	3.0±0.7	1.9±0.8	1.5±0.4	1.8±0.6
P_i, μmole/g cells	34±4	47±28	43±9	71±8	68±6

ATP, ADP, and the ATP/ADP ratio also did not change much with dilution rate and DO concentration. Inorganic phosphate (P_i) appears to have two ranges: about 40 μmole/g cells for dilution rates less than 0.2/hr and about 70 μmole/g cells

for higher dilution rates. Whether these differences in P_1 affect the kinetics is not clear at this point.

Future Direction

Experimental series S2 and S3 are underway now or are about to be started. Series S2 concerns dual limitation when the DO concentration is near 50 $\mu g/\ell$. Series S3 also is for dual limitation, but the DO concentration is near 20 $\mu g/\ell$. Once the experiments are completed, they will be interpreted with the structural model. If the model's assumptions are proven satisfactory, the model parameters will be evaluated. Finally, the model will be applied to various environmental situations to assess the effects of dual limitation.

4. TWO-DIMENSIONAL MODELING

The principal investigator for the two-dimensional modeling of nonhomogeneous aquifers containing microbial activity and sorbing substrates is A.J. Valocchi. The research assistant is Joseph Odencrantz. The work on the 2-D modeling is funded separately by a grant from Battelle Pacific Northwest Laboratory, but is closely coordinated with the DOE-supported research.

Previous Accomplishments

Modeling Capability

The First and Second Semi-Annual Progress Reports described the numerical models we have implemented for solving the two-dimensional advection-dispersion-reaction equations. Our code has a modular structure permitting the use of several alternative biodegradation submodels. For the case of single-substrate limitation (for convenience we assume here that the electron donor is limiting), the transport model is given by

$$\frac{\partial S}{\partial t} + \nabla\cdot(\mathbf{v}S - \mathbf{D}\nabla S) = -R_s \tag{4.1}$$

where S is the concentration of the limiting substrate (i.e., the electron

$$\frac{dM_t}{dt} = YR_s - bM_t \tag{4.2}$$

donor), v is the average linear velocity (pore water velocity) vector, $\underline{D}$ is the hydrodynamic dispersion tensor, R_s is the biodegradation rate term, M_t is the total active microbial mass concentration, Y is the cell yield coefficient, and b is the cell decay coefficient. Equations (4.1) and (4.2) are mass balances for S and M_t, respectively. The R_s term can be expressed by either the single-substrate Monod equation

$$R_s = M_t q_m \left(\frac{S}{K_s+S}\right) \tag{4.3}$$

or the biofilm kinetic submodel

$$R_s = aJ(S) \tag{4.4}$$

where q_m is the maximum rate of substrate utilization, K_s is the half velocity constant for the electron donor, J is the substrate flux into the biofilm, and a is the specific surface area of the biofilm The biofilm kinetic submodel rigorously couples external mass transfer resistance with simultaneous diffusion and reaction within the biofilm. Thus, J is a complex nonlinear function of S which is determined from equations presented by Rittmann and McCarty (1981). Additional details about our implementation of biofilm kinetics are given in the Second Semi-Annual Progress Report.

For the case of dual-substrate transport and reaction, Eqns. (4.1) and (4.2) must be supplemented by a mass balance for the second substrate, which is here assumed for convenience to be the electron acceptor. This additional transport equation is

$$\frac{\partial A}{\partial t} + \nabla\cdot(\mathbf{v}A - \underline{D}\nabla A) = -R_A \tag{4.5}$$

where A is the concentration of the electron acceptor and R_A is the biodegradation rate term. Several options for the R_S and R_A terms have been implemented in this case. One possibility is the multiplicative dual Monod expression,

$$R_S = M_t q_m \left[\frac{S}{K_S + S}\right] \left[\frac{A}{K_A + A}\right] \tag{4.6}$$

$$R_A = \gamma R_S \tag{4.7}$$

where K_A is the half velocity constant for the electron acceptor and γ is a stoichiometric coefficient. Another possibility is the so-called "minimum-rate" single Monod expression, which has the form

$$R_S = M_t q_m \left[\frac{S}{K_S + S}\right], \quad R_A = \gamma R_S \tag{4.8}$$

if S limits, or

$$R_A = M_t q_m \left[\frac{A}{K_A + A}\right], \quad R_S = \gamma R_A \tag{4.9}$$

if A limits. The final option is a "minimum-rate" biofilm kinetic submodel where

$$R_S = aJ(S), \quad R_A = \gamma R_S \tag{4.10}$$

if S limits, or

$$R_A = aJ(A), \quad R_S = \gamma R_A \tag{4.11}$$

if A limits.

A summary of our current modeling capabilities is given in Table 4.1.

Table 4.1 Optional Biodegradation Rate Expressions Available in the Two-Dimensional Transport Code

	Monod			Biofilm	
	single	multiplicative	minimum-rate	single	minimum-rate
single substrate transport	X			X	
dual substrate transport		X	X		X

The modular nature of our code is made possible by the operator time splitting (OS) technique used to solve the coupled transport and reaction equations. OS splits the reactive transport equations (4.1) and (4.5) into a nonreactive transport partial differential equation and a reaction ordinary differential equation. The nonreactive (two-dimensional) advection-dispersion equation is solved by the Principal Direction Finite Element Method (PDFEM) of MacQuarrie et al. (1989) and the reaction equation is solved by a standard fourth-order Runge-Kutta method. Additional fundamental material on OS is given by Wheeler and Dawson (1987) and Wheeler (1988). The Second Semi-Annual Progress Report contains the details about our implementation of OS, as well as an extensive analysis of the accuracy and efficiency of our code.

Numerical Simulations to Compare Biofilm and Monod Kinetics

An example problem comparing biofilm and Monod degradation kinetics was described in the Second Semi-Annual Progress Report. Although those results showed that Monod kinetics gave substantially faster substrate removal, we subsequently discovered a units error in our simulations. Corrected results are reported below.

Progress

Modeling Developments

Although the development and testing of our codes is complete, we continue with refinements and modifications. The biomass-balance equation was modified to describe more realistically what happens to existing biomass before substrate reaches it. In the original model formulation, biomass decays with specific rate b. This leads to a depletion of biomass for regions not yet contacted by exogeneous substrate. However, the reality is that background biomass levels exist and do not decay away. To eliminate the unrealistic decay of background biomass, the biomass-balance equation (4.3) was changed to

$$\frac{\partial M_t}{\partial t} = YR_s - bM_t + bM_{to} \tag{4.12}$$

in which M_{to} = initial (or background) biomass density.

Comparison of Biofilm and Monod Biodegradation Kinetics

Figure 4.1 shows the domain, source location, boundary conditions, and transport parameters used to reevaluate the comparison of Monod and biofilm kinetics. The same initial biomass density of 10^6 cells/g of dry medium was used in both cases; this represents an intermediate value found in natural aquifers. Other biofilm parameters specified in Fig. 4.1 include X_f, the biofilm density, D_m and D_f, the molecular diffusivity in the pore water and biofilm, respectively, d_p, the particle diameter, and L, the external diffusion layer thickness. Hydrodynamic parameters specified in Fig. 4.1 include v_x, the pore water velocity, ϵ, the porosity, and α_L and α_T, respectively the longitudinal and transverse dispersivities.

The domain initially contains none of the single rate limiting substrate, which is input at the source location shown in Fig. 4.1. Plumes of the substrate and biomass develop downstream of the source. Typical results for the case of

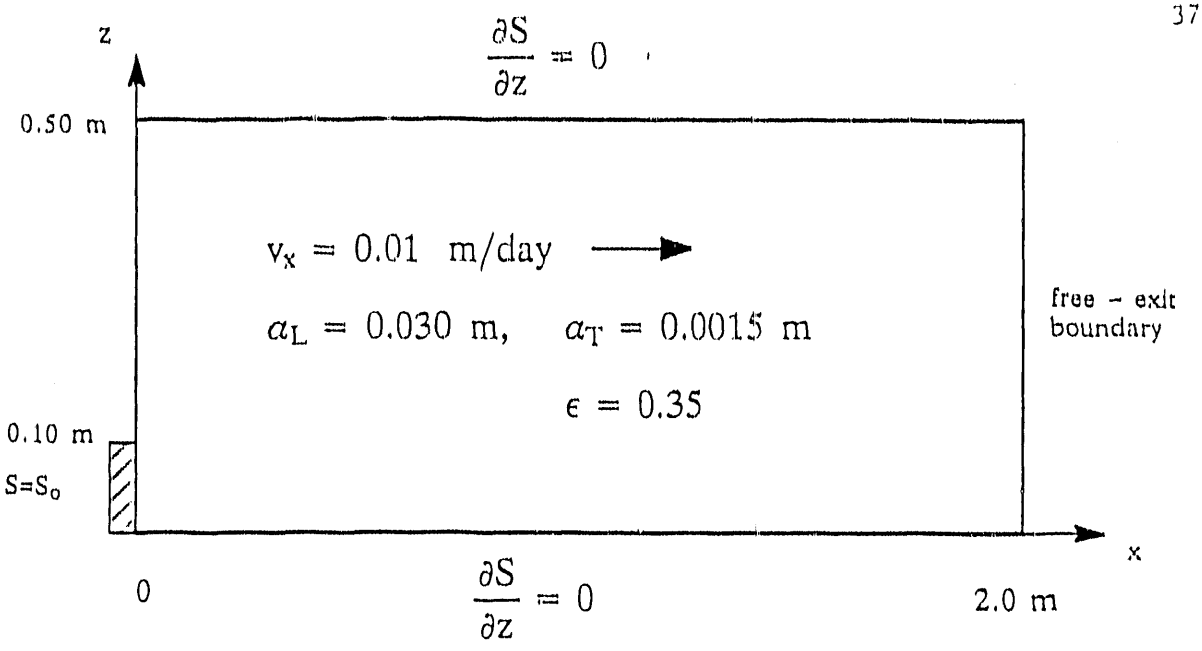

Kinetic Parameters

Monod

q_m = 0.420 mg SOC/mg cell-day
K = 0.218 mg/L
Y = 0.678 mg cells/mg SOC
b = 0.07 day $^{-1}$

Biofilm

q_m = 0.420 mg SOC/mg cell-day
K = 0.218 mg/L
Y = 0.678 mg cells/mg SOC
b = 0.07 day $^{-1}$
X_f = 0.15 mg cells/cm^3
D = 1.07 cm^2/day
D_f = 0.856 cm^2/day
d_p = 0.10 cm
L_{fo} = 0.0598 μm
L = .770 cm

PDFEM and Operator-Splitting Parameters

Δx = 0.027m
Δz = 0.020m
Δt = 1.0 day

Peclet # = 0.89
Courant # = 0.375
ϱ_1 and ϱ_2 = 0.422 - .0375
Runge - Kutta Steps = 20

Figure 4.1 Domain and parameters used for single-substrate limitation simulations in homogeneous porous media.

biofilm kinetics are displayed in Fig. 4.2 which shows the substrate plume at 13.2 days and 26.4 days; the biomass and substrate distributions are qualitatively similar. The results at the time of 26.4 days are approximately at steady state. At early times the plume penetrates far into the domain and there is a correspondingly extensive region of biomass growth. However, as time progresses, the biomass builds up closer to the source and the resultant increase in the degradation rate causes the plume to retreat and diminish in size. An overall picture of the simulation results is shown in Figs. 4.3 and 4.4, which are plots of the total mass of substrate and biomass in the domain versus time.

The key issue is how the previous results compare with those for the case of Monod kinetics. In this case, the results are virtually identical. This is because the biofilm thickness is so small that there is no effect of internal mass transfer limitation caused by molecular diffusion within the biofilm. When both internal and external mass-transfer resistances are small, the biofilm and Monod submodels are identical. Hence we also must conclude that external mass-transfer limitation is negligible in this case.

An important question is how general is the above conclusion. The relative importance of internal and external mass-transfer phenomena has been quantified by Suidan et al. (1987). A dimensionless biofilm thickness can be defined by

$$L_f^* = \frac{L_f}{\sqrt{\frac{2K_s D_f}{q_m X_f}}} \tag{4.13}$$

and a dimensionless external film thickness by

$$L^* = \frac{L}{\sqrt{\frac{2K_s D_f}{q_m X_f}}} \tag{4.14}$$

Suidan et al. (1987) showed that biofilms are fully penetrated for $L_f^* \leq 0.2$

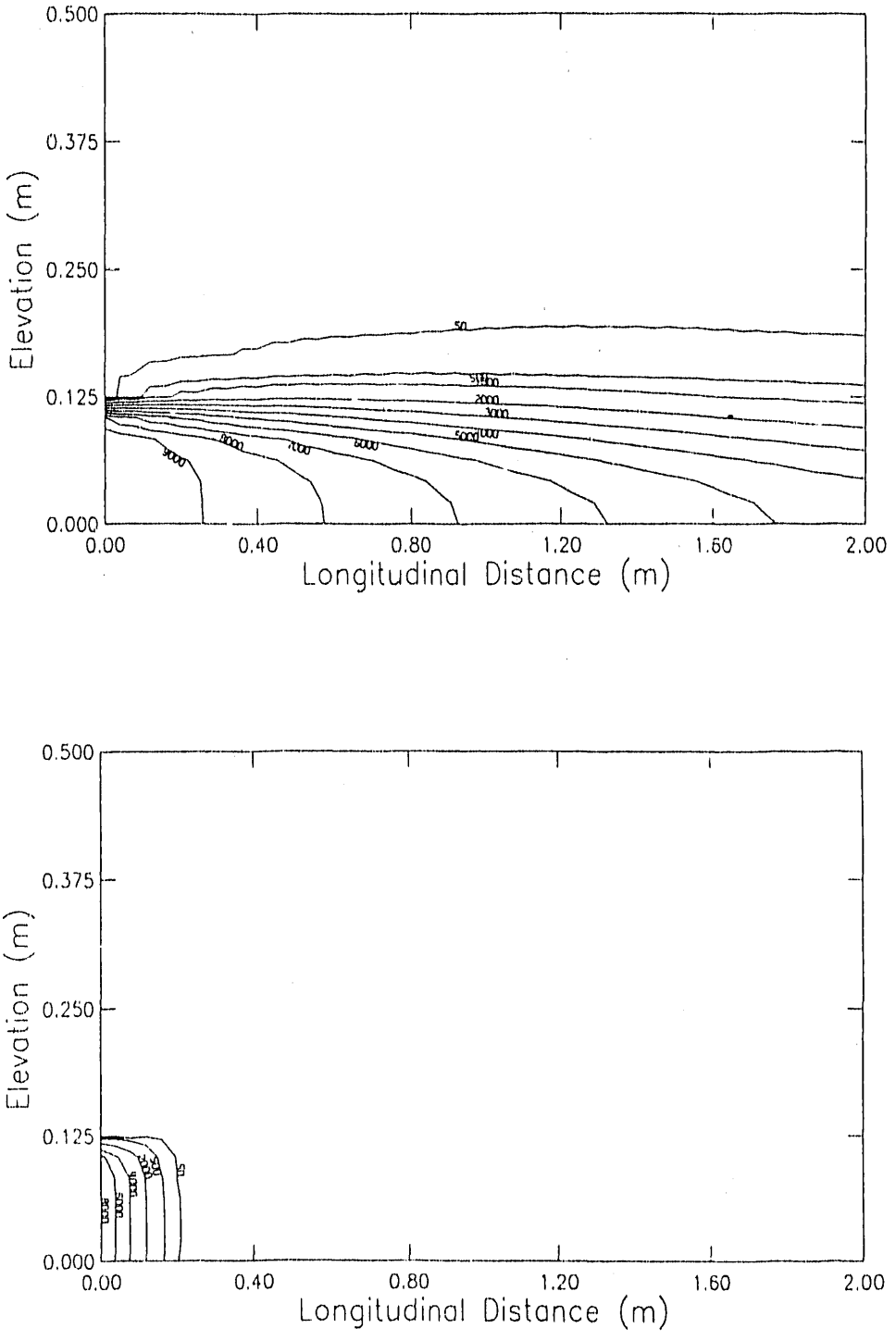

Figure 4.2 Contour Plots of the organic substrate compound at 13.2 days (top) and 26.4 days (bottom). The concentration is expressed in mg/ℓ.

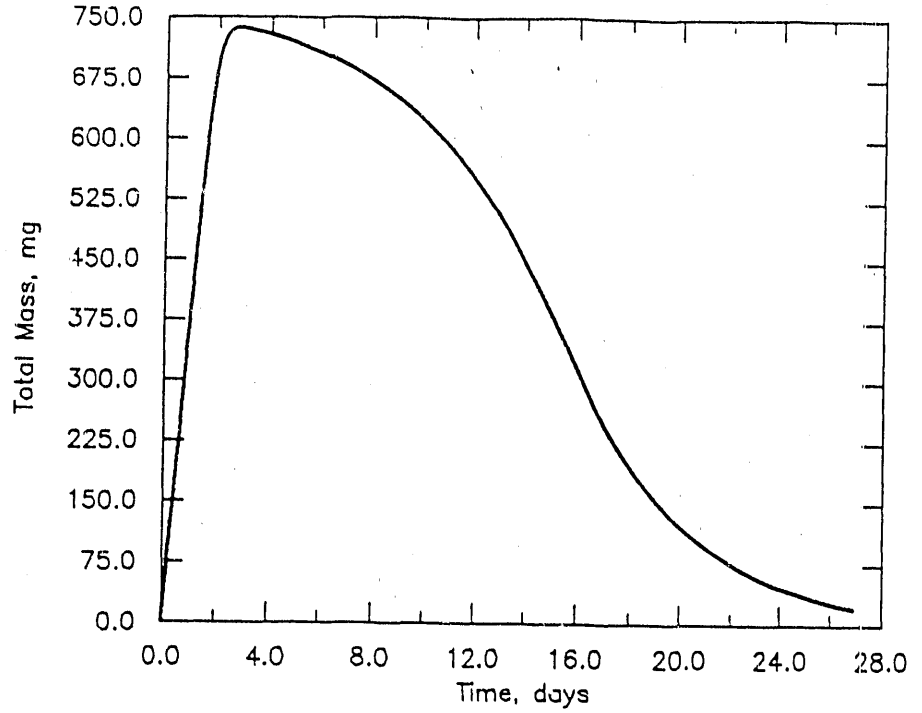

Figure 4.3 Total organic substrate mass in the system versus time throughout the simulation.

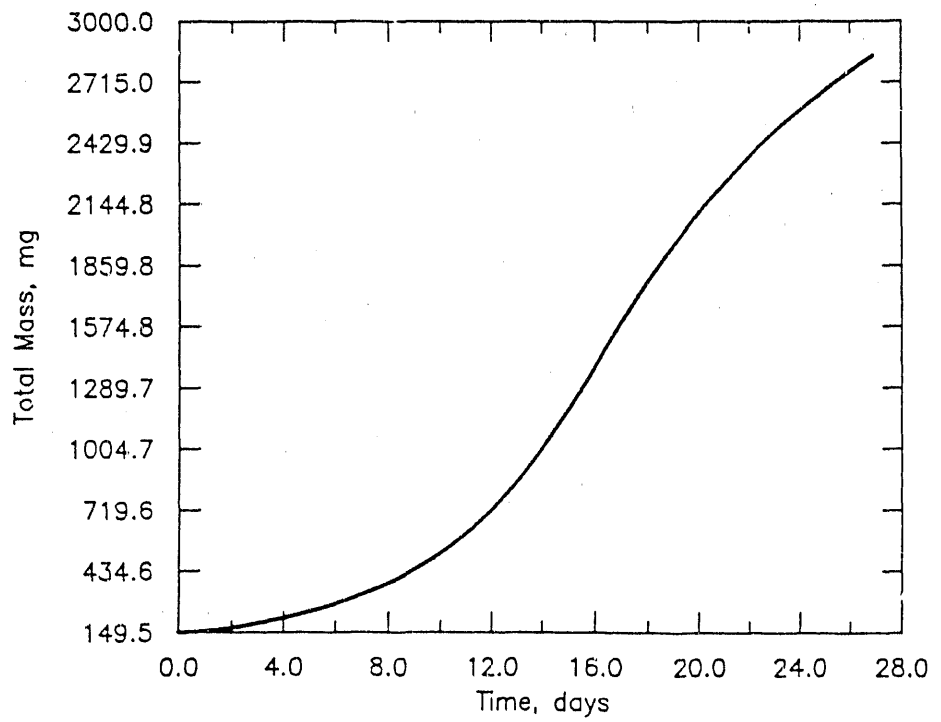

Figure 4.4 Total biomass in the system versus time throughout the simulation.

(i.e., no internal gradient within the biomass). Thus, biofilm effects will be more evident when L_f^* is increased, such as by increasing substrate inputs to increase L_f, decreasing K_s, or increasing q_m or X_f. In the situation presented here, L_f^* is very small (L_f^* never exceeded 0.011 at steady-state). External mass-transfer resistance is negligible when $L^* < 0.01$ (Heath et al., 1990). There is great uncertainty in estimating L for real soils. There are numerous empirical models available in the literature to estimate the diffusion layer thickness for defined ranges of Reynold's number. Nicoud and Schweich (1989) note that these models provide drastically different values at low Reynold's number and suggest that more research is needed to predict the magnitude of external mass transfer coefficients. Here the diffusion layer thickness was estimated to be 0.18 mm, which corresponds to a dimensionless diffusion layer thickness of 2.3. Although this represents a moderate amount of external mass transport resistance, it was shown to have a negligible impact for this simulation.

Comparison of Multiplicative and Minimum-Rate Monod Biodegradation Kinetics

There is some controversy in the literature regarding the proper kinetic model for the case of dual-substrate limitation. We have conducted several numerical experiments to evaluate the differences between the multiplicative Monod (Eqns. 4.6 and 4.7) and the minimum-rate Monod (Eqns. 4.8 and 4.9) models. Transport simulations in a domain similar to that in Fig. 4.1 are being conducted for a variety of kinetic parameter values. Details will not be presented here. Our preliminary results indicate that significant differences between the two kinetic formulations exist when the half-velocity coefficients are on the same order of magnitude as the substrate input or background concentration.

Numerical Experiments in Stratified Porous Media

We have begun to conduct simulations in stratified porous media in order to examine the influence of heterogeneity on coupled transport and biodegradation

processes. Figure 4.5 shows the problem definition we have used in our work to date; the system consists of two layers with mass input along the entire influent boundary. Kinetic parameters are the same as those listed in Fig. 4.1. We have performed single- and dual-substrate transport studies using Monod biodegradation kinetics. We will present some preliminary results for dual-substrate transport with multiplicative Monod kinetics.

At time zero there is a uniform background concentration of electron donor present but no electron acceptor. The acceptor (but no donor) is continually input into the domain as shown in Fig. 4.5. Figure 4.6 shows the distribution of donor, acceptor, and biomass at time 1.65 days. The donor has almost migrated completely out of the fast (top) layer and any subsequent removal in the fast layer results from transverse dispersion of donor from the slow (bottom) layer. There is some significant biomass growth and decay in the slow layer in the region of the dispersed donor/acceptor front (note that the multiplicative Monod equation requires both donor and acceptor to be present for degradation to occur) and also downstream near the layer interface due to transverse dispersion of the acceptor from the top layer. The layer interface is a region of enhanced biological activity and it is interesting that the transverse spread of the biomass about the interface is significantly greater than that of the donor and acceptor. The "looped" contour of biomass protruding into the upper layer is a transient condition resulting from growth near the interface and decay in the fast layer away from the interface.

It is apparent that transverse dispersion plays a major role in controlling the overall amount of biodegradation in the stratified system described above. This is confirmed by other numerical experiments where we have varied the longitudinal and transverse dispersivity. At this time we have not completed our analysis of the results; however, in general, the total removal of the donor

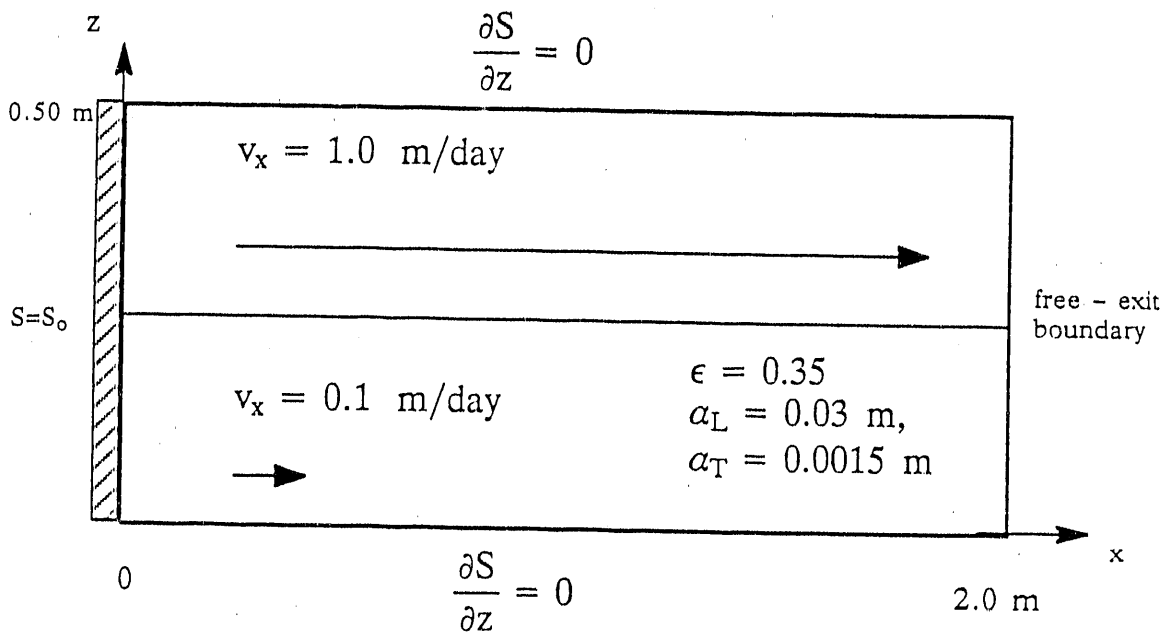

Top Layer	Constant	Bottom layer
Pe = 0.886	$\Delta x = 0.027$m	Pe = 0.86
Co = 0.375	$\Delta z = 0.01923$m	Co = 0.0375
$\rho_1 = 0.423$	$\Delta t = 0.011$ day	$\rho_1 = 0.0436$
$\rho_2 = 0.040$	Total Nodes = 2052	$\rho_2 = 0.00642$
	Runge - Kutta Steps = 50	

Figure 4.5 Domain and parameters used for the simulation in stratified porous media.

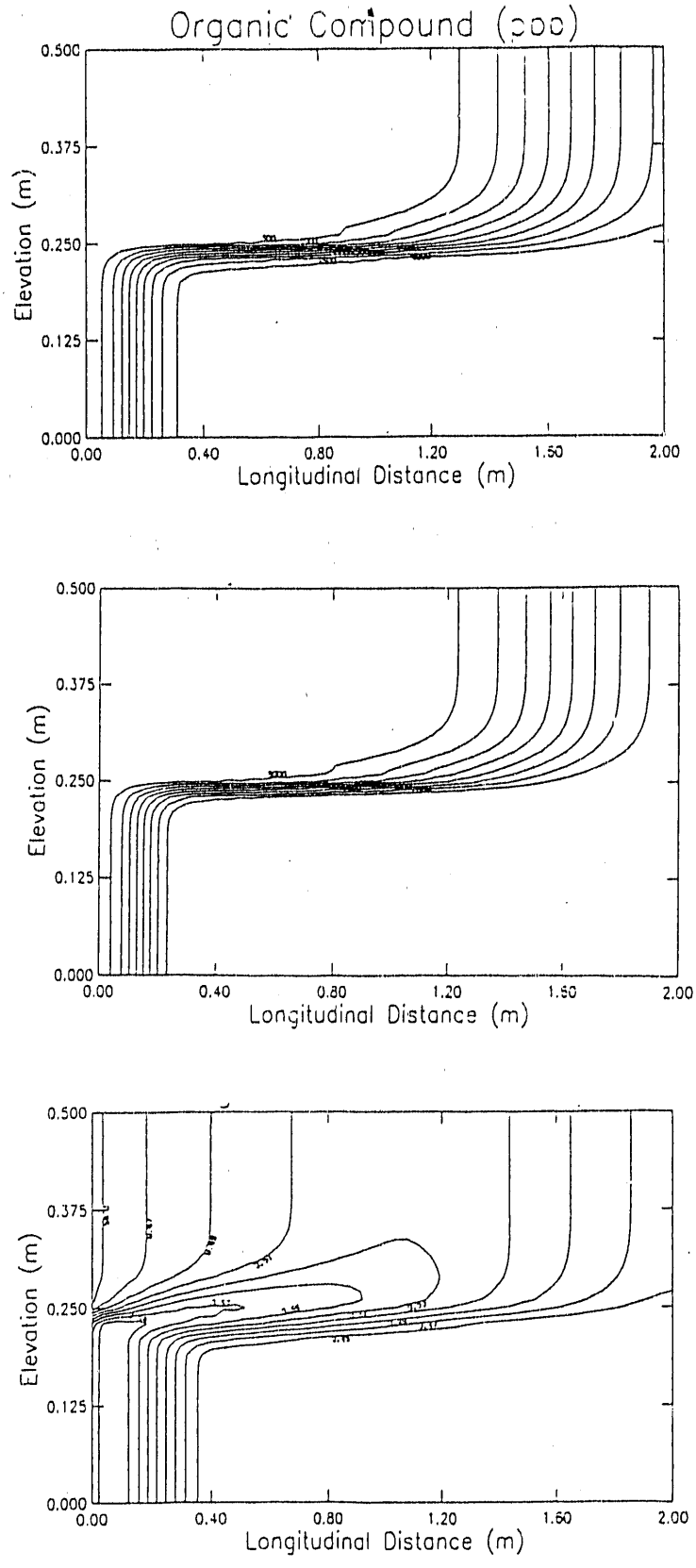

Figure 4.6 Contour plots of the donor (top), acceptor (middle), and biomass (bottom) at 1.65 days. The units for the donor and acceptor are mg/ℓ and for the biomass are μg/ℓ.

increases with dispersivity.

Future Directions

In the near future, we plan to focus upon numerical experiments for stratified porous media. We will continue to examine systematically the impact of the physical and biological parameters, as well as the number and thickness of the layers. We also plan to study the impact of adsorption of the donor. For the stratified case reported above, adsorption could have a significant influence since retardation of the donor would provide much greater contact time between donor and acceptor.

5. BACTERIAL CLOGGING BY STRICTLY AEROBIC BACTERIA

The principal investigator is Dr. P. Baveye of Cornell University. The research assistants are Philippe Vandevivere and Diego de Lozada. The objective of the research is to determine the mechanisms by which aerobic chemoorganotrophic bacteria clog porous media. Diego de Lozada's work focuses upon determining whether and under what conditions gas accumulation may cause clogging. Laboratory techniques encompass column percolation studies and direct microscopic observation via scanning electron microscopy.

Previous Accomplishments

Two bacterial species were chosen. The first is Bacillus subtillis, which is reported to produce large amounts of polysaccharide slime. The second species is Arthobacter sp., which is an actinomyate that grows on gaseous hydrocarbons. Initial experiments were conducted with B. subtillis.

Initial experiments in a simple sand column permeameter showed a sudden onset of clogging that reduced the hydraulic conductivity to 0.1 to 0.5% of the initial value. Most of the clogging occurred in the first 3 cm. Scanning electron microscopy of sand samples taken with a special corer showed B. subtillis growing in head-to-tail chains. A preliminary hypothesis was that

the chains extend into the flowpath and increase drag.

In the second semi-annual progress report, an improved permeameter was described. It makes sterilization, sampling, head-loss calculation, and medium oxygenation much easier. Most importantly, clogging of the inlet mesh was avoided by placing the inoculum 0.8 cm downstream of the mesh.

A method to sample, fix, dehydrate, and store intact core samples was developed. All reactions occur within the corer. Solidified sample is extruded, sectioned, sublimated, and prepared for SEM.

Permeameter studies with B. subtillis and Arthrobacter showed gradual loss of hydraulic conductivity within the first 3 cm when low glucose concentrations were fed (5-100 ppm). SEMs showed little extracellular polymer, and the cells grew as microcolonies. One reasonable hypothesis for clogging is that detached bacteria accumulate at the pore throats; although the total biomass is not high, its accumulation at throats can accentuate its effects on permeability.

Bacterial clogging by strictly aerobic bacteria: Pure culture studies *with Arthrobacter ssp.*

This section summarizes data obtained since the first annual report related to the reduction of the saturated hydraulic conductivity, K_s, of sand columns by *Arthrobacter ssp*. These experiments involve, on the one hand, determinations of biomass distributions within the sand columns and their correlation with K_s values and, on the other hand, the use of a nutrient solution that causes the cells to excrete slime inside the sand columns in order to assess the role of such excretions in clogging. A manuscript summarizing the results obtained to date on the clogging of porous media by aerobic chemoorganotrophic bacteria will be submitted shortly to SSSAJ (Vandevivere and Baveye, 1990).

Methods

Treatments: We ran 4 permeameters continuously for up to 40 days. Two treatments have been applied with two replicates for each each treatments. The first treatment consisted in two columns that were percolated with a nutrient solution having the same composition as described in the second semi-annual report (with 20 mg/L of glucose) except that no oxygen was added to the solution since the air-saturated concentration provides enough oxygen for the oxidation of this amount of glucose. As demonstrated in the second semi-annual report, this medium is glucose-limited. The two other columns were percolated with a solution of the same composition except that the nitrate salt concentration was decreased to make a nitrogen-limited medium. Thus the first treatment is C-limiting with a C/N ratio of 2.4 while the second treatment is N-limiting with a C/N ratio of 48 for the first 23 days and of 96 thereafter.

Inoculation: The experimental set-up is as described in the last report. One difference, however, is the point of injection of the inoculum. The bacterial suspension was injected at a depth of 2 cm from the inlet mesh instead of 0.8 cm, since this latter distance does not seem sufficient to prevent back migration of the cells to the inlet mesh during the experiments.

Scanning electron microscopy: We described earlier a sampling-preparation procedure (Peldri embedding) that enables us to view assemblages of sand particles without disrupting their structure. We also reported that the bacteria were very well preserved using that technique. Further investigation of this technique led us, however, to revise our viewpoint. Although the Peldri embedding technique preserves the structure of individual bacterial cells at least as well as the critical-point-drying technique, the technique causes clumping of the cells in dense aggregates. Since this artifact is probably produced during the solidification step, we attempted to avoid it by increasing

the solidification rate with liquid nitrogen. It did not solve the problem and the Peldri method was abandoned. We therefore switched back to the sampling method described in the first semi-annual report. The reported problem of the sand core disintegrating upon its extraction from the micro-sampler can in fact be solved very simply. Instead of extracting the whole core and then mounting it, we extrude it partially (using a small piston) and mount the exposed section by pressing it on a piece of tape and repeat the operation to obtain deeper sections.

Since the presence of slime in the N-limited columns was evinced by light microscopy and since the conventional preparation of samples prior to SEM analysis fails to preserve well the ultrastructure of slime layers, we adapted for the SEM a TEM procedure proposed by Boyles (1984) to improve the chemical fixation of glycocalyces and other types of organelles. This procedure involves a prefixation step with L-lysine and glutaraldehyde (mixed immediately before use).

Distribution of biomass: At the end of a run, the distribution of biomass density in a sand column is measured by sampling a core and assaying the phospholipid concentration in subsamples of the core. It is not possible to convert the phospholipid concentration into a number of cells because cells have a variable phospholipid content depending on their physiological state (size). However, the phospholipid to cell volume ratio is constant throughout the growth curve. Therefore, with the appropriate conversion factor determined for a batch culture, the phospholipid concentration can be expressed as volume of the cells per unit volume of porous medium or as the percentage of the pore space that is occupied by the cells.

Alternatively, considering the low variability of the mass density of bacterial cells, we may compute from the phospholipid concentration the mass of

bacterial cells per unit volume of porous medium.

Results and discussion:

The distribution of the biomass in the four permeameters that were described in the last report (inoculated with *Arthrobacter ssp.* and operated under constant flux conditions) is shown on Fig. 5.1. These biomass data correlate well with the conductivity data (reported earlier), in that high biomass densities correspond to low K_s values.

Figures 5.2 and 5.3 show the evolution with time of the hydraulic conductivity, averaged over the entire permeameter, for the C-limited and N-limited treatments, respectively. Included in Fig. 5.3 is a curve from a previous experiment carried out under the same conditions, except that oxygen was added (curve ending on day 20). It appears that as a result of decreasing the nitrate concentration in the feed, the saturated hydraulic conductivity, K_s, reaches a plateau after 18 days of flow, whereas with a normal supply of nitrate (C-limited columns), K_s is still decreasing at the end of the experiments, i.e., after 35 days of flow. When the nitrate concentration is even further reduced (day 23), instead of limiting further the clogging effect, it suddenly enhances it. K_s was further reduced by a factor of 1.7 and 2.7 for the two replicates. At the same time (day 23), the bacteria observed in the interstitial liquid sampled with a sterile syringe, switched from a nonencapsulated to an encapsulated form (a process that roughly quadrupled their volume). The production of a bacterial capsule may be a consequence of an overflow metabolism, i.e., a surplus of cellular energy and carbon sources relative to nitrogen availability. This overflow metabolism stems from the fact that the populations whose nitrogen supply was decreased so drastically do not down-regulate their respiratory activity.

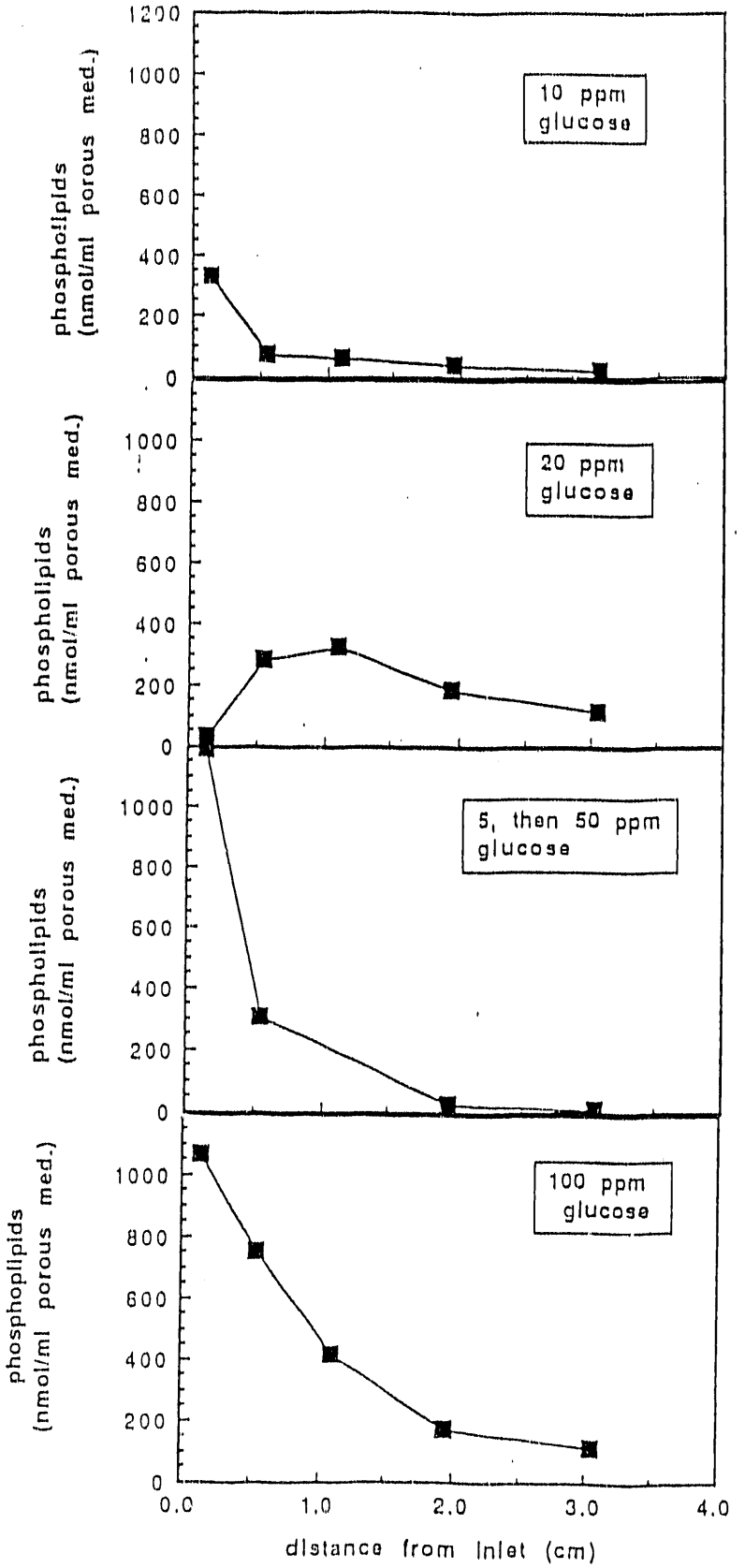

Figure 5.1 Profiles of bacterial density in 4 C-limited permeameters.

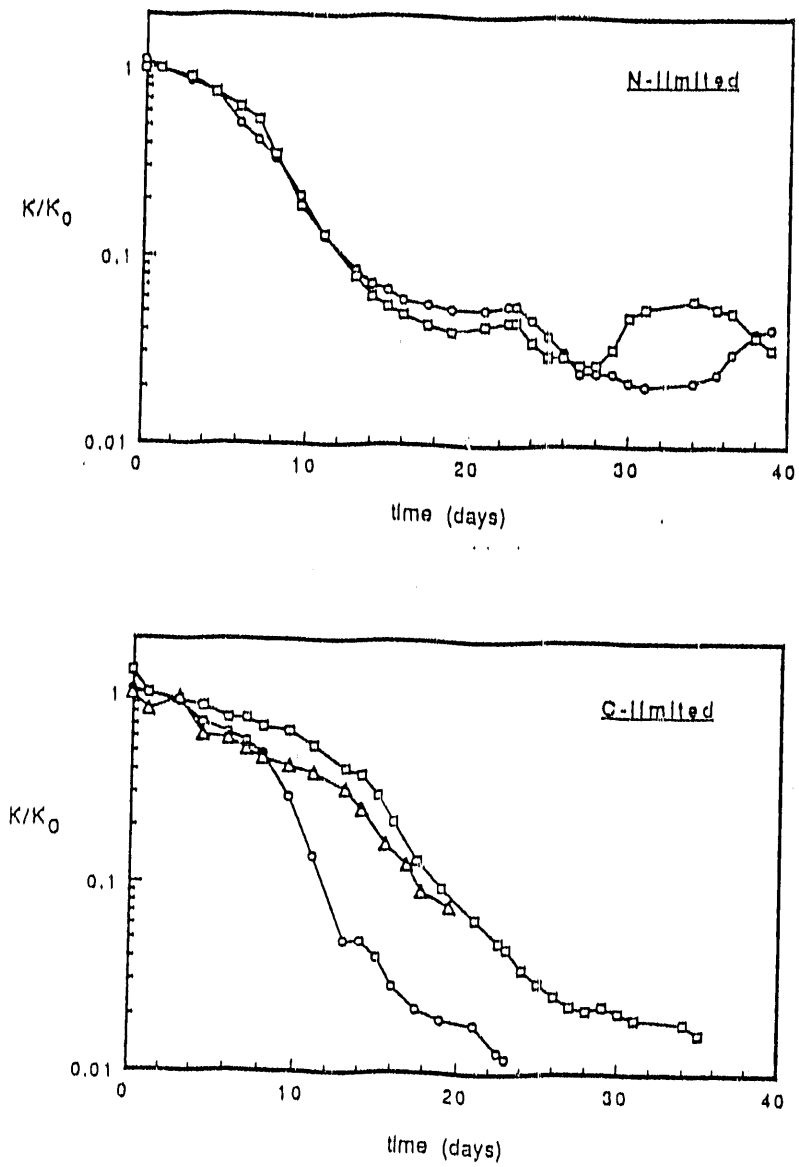

Figures 5.2 and 5.3. Evolution of the hydraulic conductivity of the N-limited and C-limited permeameters.

C-limited: 20 mg/L glucose, 30 mg/L KNO_3
N-limited: 20 mg/L glucose, 1.5 mg/L KNO_3
and 0.75 mg/L KNO_3 after day 23.

The reduction of K_s brought about by the nitrogen deficiency is unstable (Fig. 5.2). After a while the system returns to the previous steady state. In one of the N-limited columns, K_s resumes declining on day 36. This was caused by the colonization and plugging of the inlet mesh (Fig. 5.4).

Figures 5.4 and 5.5 show the profiles of hydraulic conductivity, bacterial density and dissolved oxygen for the N-limited and C-limited permeameters, respectively. The biomass distribution is bimodal, except in the case of column c which was sampled sooner. The main peak is located slightly before the point of injection of the inoculum. The second peak, at the inlet, reflects the ability of our strain (nonflagellated) to move against the general direction of flow and to reproduce very fast at the inlet interface. It took exactly 34 days for the cells in the two N-limited replicates to reach and clog the inlet mesh distance by 2 cm from the point of injection, while it took 29 days for the same to happen in the case of the C-limited column. As the cells move up against the general direction of the flow, they induce clogging of the areas newly colonized in the case of N-limitation (Fig. 5.4) but fail to do so when C-limited (Fig. 5.5). In any case, when the cells reach the inlet mesh, they clog it very rapidly.

In permeameters a, b, and c, clogging goes on beyond 2 cm after the 10th day while there is no apparent respiratory activity (Figs. 5.4 and 5.5). This could suggest a mechanism of biomass detachment in regions closer to the inlet, entrainment, and filtration in deeper layers causing reductions of K_s without apparent respiratory activity.

The biomass density (phospholipid concentration) at steady state is not affected by the decrease of the nitrogen supply (Figs. 5.4 vs. 5.5).

The undisturbed samples from all permeameters, when fixed conventionally with glutaraldehyde and viewed under the electron microscope, show naked cells

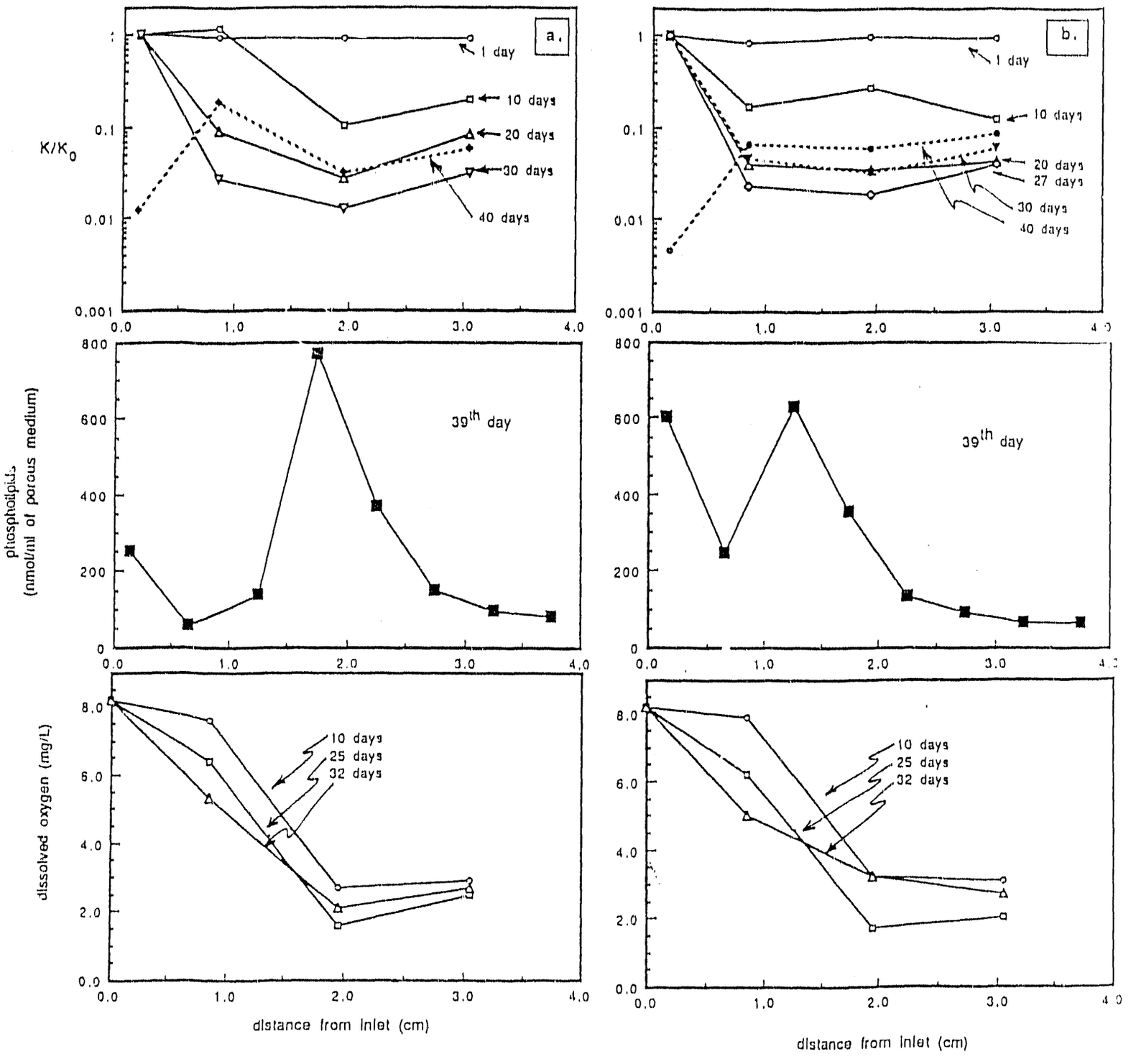

Figure 5.4 Profiles of hydraulic conductivity, biomass, and dissolved oxygen at different time intervals in the 2 permeameters fed with an N-limited nutrient solution. Arrow indicates the injection point of the inoculum.

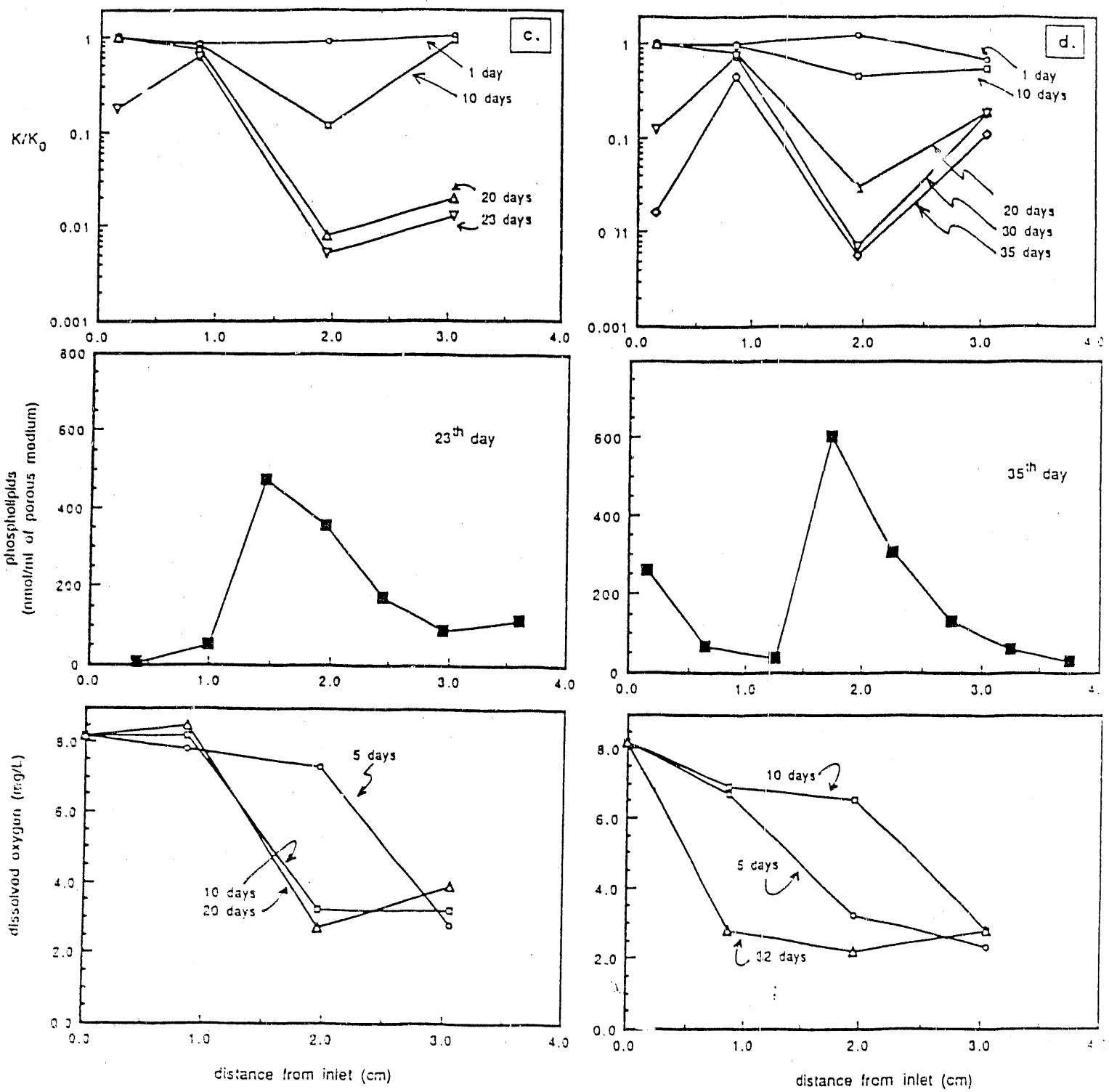

Figure 5.5 Profiles of hydraulic conductivities, biomass, and dissolved oxygen at different time intervals in the 2 permeameters fed with a C-limited nutrient solution. Arrow indicates the injection point of the inoculum.

forming loose three-dimensional aggregates without any extracellular material. In the N-limited columns, where the presence of capsular EPS had been detected by light microscopy, a dense meshwork of fibrils extends between the cells. This feature of the N-limited columns may explain the enhanced clogging on and after day 23.

The data for K_s reductions and the biomass accumulation (expressed as biomass per unit volume of the porous medium) are plotted in a $\log_{10}$-$\log_{10}$ graph in Fig. 5.6. To summarize the results mathematically in a way that might be used in computer simulations, we have tried a number of functional relations. The equation $y = \exp(-0.335\ x^{0.85})$, where y is the relative K_s ($= K_s/K_{so}$) and x is the biomass density, seems to capture best the essential features of the data. In particular, it reproduces well the acceleration in K_s reduction that occurs at biomass density values above 5 mg/cm^3 which corresponds to an occupation by the cells of about 1% of the pore space. When this occupation reaches 7%, the reduced Ks is decreased by three orders of magnitude. Even though the above equation is purely descriptive, it would be interesting to use it in 2-D simulations of solute transport to study the spatial effect of clogging on the transport pattern in the vicinity of injection wells.

Conclusions

Aerobic bacteria can reduce K_s very severely (3 to 4 orders of magnitude) in less than a week. This K_s reduction is associated with the formation of a thick, though highly porous, bacterial mat on the inlet face of the sand column. When the formation of such a mat is prevented, K_s reduction occurs at a much slower rate inside the sand column.

Though the K_s reduction inside the sand can be slowed down by decreasing the carbon supply and be stopped by reducing the nitrogen supply, mat formation and inlet clogging develop very rapidly even at relatively low glucose

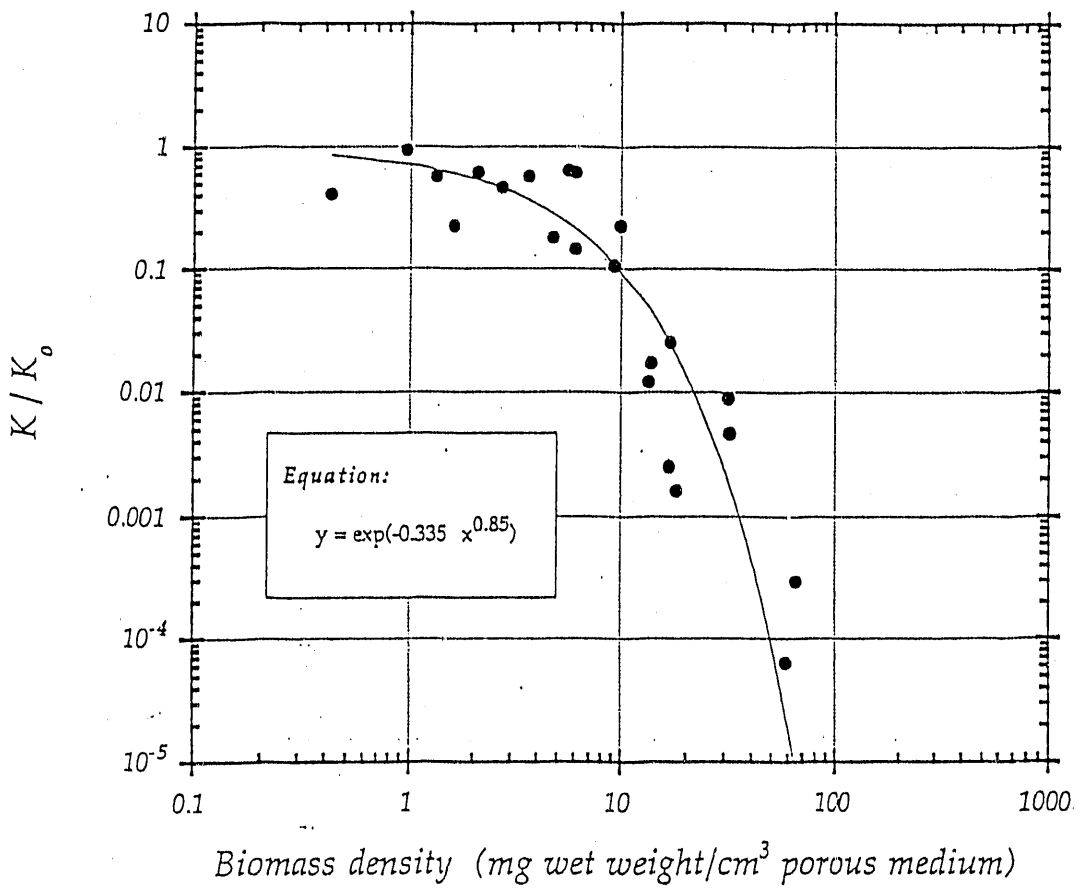

Figure 5.6 Evolution of the reduced saturated hydraulic conductivity as a function of bacterial density. (Data points are taken from all permeameters in layers where no channeling was apparent as evidenced by a horizontally uniform hydraulic head at both ends of the layer)

concentration (10 mg.L-1). EPS were produced and seemed to cause additional reduction of K_s when the C/N ratio of the nutrient solution was high (100). At lower C/N ratios (smaller than 50), EPS were absent of clogged layers as revealed by light and electron microscopy and the cells themselves seemed solely responsible for the decrease of K_s.

Bacteria do not form biofilms in the sand columns. Instead of forming 2-D coatings on the surfaces of sand particles, bacteria grow in the pore space where they form large spherical aggregates that create local plugs in the flow channels.

Clogged layers are always very shallow (less than 1 cm thick) and are characterized by a high bacterial density. Even with convective flux (average pore velocity of 0.1 $mm.s^{-1}$), nutrient depletion occurs readily along the flow path. These results stress the need for slightly recalcitrant substrates in bioremadiation schemes as was suggested by McLeod et al. (1988).

Bacterial Clogging by Strictly Aerobic Bacteria: Mixed cultures of DOE SMCC collection isolates and protozoa

The second part of this section describes preliminary results of experiments involving mixed cultures of DOE SMCC (Subsurface Microbial Culture Collection) isolates and protozoa. In order to find out if the conclusions reached with the two strictly aerobic bacteria studied so far, i.e., *Bacillus subtilis* and *Arthrobacter spp.*, apply to other aerobic strains that are likely to play an active role in biostimulated aquifers, we are preparing new experiments with bacterial isolates from the SMCC collection. Prof. Balkwill kindly provided us with 10 strictly aerobic bacterial strains from the Savannah River Site. Since one of the crucial points is to find out if extracellular substances are actually produced and accumulated in natural porous media and what their impact on K_s might be, we chose to work with SMCC isolates that are the

most likely to catalyze such a reaction, i.e., strains that form mucoid colonies on PTYG agar.

Another step was taken to bring our experimental system closer to natural systems. Protozoa are common inhabitants of aquifers. These eukaryotes are able to decimate bacterial populations and therefore have the potential to affect the role played by bacteria as clogging agents. We plan to assess that potential by conducting some experiments with mixed cultures of bacteria and protozoa.

Bacterial and protozoan strains:

Based on the criteria of strict aerobicity (lack of glucose fermentation and lack of nitrate reduction for the API Rapid NFT test) and exopolysaccharide, or EPS, production (mucoidness of colonies), the following bacterial isolates from the DOE SMCC collection were selected: A0393, B0693, B0577, B0579, and B0649 from the Middendorf formation (at depths ranging from 709 to 851 ft), B0422 and B0428 from the Pee Dee formation (at 477 ft depth), B0550 and B0483 from the Black Creek formation (at 668 ft depth) and B0121 from the Ellenton formation (at 387 ft depth). These isolates were obtained at Florida State University from Savannah River Site drilling sites P28 (strain A-) and P24 (strain B-) in June-July 1986.

The protozoan strain was bought from the ATCC collection since no pure isolate from the DOE program seems to be available at the moment. We chose the strain *Acanthamoeba terricola* ATCC 30134 isolated from arable soil. It belongs to the class of Mastigophorae (Amoebae), is of small size (20 to 30 micrometers in diameter), forms cysts and is commonly encountered in soil environments. This amoeba can grow in the absence of bacterial cells by ingestion of soluble organic compounds. The medium used to maintain the protozoa and to prepare inocula (PYG) is made by mixing proteose peptone (20 g), yeast extract (1 g), agar if needed (20 g), distilled water (900 mL), 0.4M $Mg.SO_4.7H_2O$ (10 mL), 0.05M $CaCl_2.2H_2O$

(8mL), sodium citrate dihydrate (1g), 0.005M $Fe(NH_4)_2(SO_4)_2.6H_2O$ (10mL), 0.25M $Na_2HPO_4.7H_2O$ (10 mL), 0.25M KH_2PO_4 (10mL), and 2M glucose (50 mL). The pH is adjusted at 6.5.

Growth on defined medium:

The bacterial strains are maintained on PTYG (Peptone-Tryptone-Yeast extract-Glucose) agar. Growth on a defined medium is desired in the context of our experiments since organic colloids present in this complex medium may precipitate in the columns and complicate the analysis of the data. Therefore we tested the ten bacterial isolates for growth on the defined medium used up to here in our percolation experiments (see second semi-annual progress report, March 1990). All but two strains (A0393 and B0121) were able to grow on this defined medium devoid of any growth factor. The experiments described hereafter were performed on the eight strains that can multiply in the defined medium.

EPS formation and motility:

Two important traits affecting the behavior of bacteria in porous media are motility and type of EPS produced. Motility of the eight strains that were selected on account of their ability to grow on the defined medium, was checked by observation with a light microscope. Observation was made on young cultures grown in the defined medium. Only one strain, B0579, was motile under these conditions.

EPS excretions can remain attached to the cells and form a geometrically well-defined capsule or disperse in the medium in so-called slime layers. Some strains can produce both types of EPS. The type of EPS excretions produced by the eight isolates was observed with a light microscope in a thin wet mount negatively stained with China ink. At the exception of B0579, all strains produce a capsule and only negligible amounts of slime layers when grown in the defined medium (liquid, shaken). The strain B0579 does not produce EPS at all

when grown for 3 days in the defined medium.

Susceptibility to protozoan feeding:

Since we want to assess the influence of prey-predator relationship between bacterial and protozoan populations, the occurrence of predation should first be observed (certain bacterial strains are resistant to certain protozoans). Two procedures were followed to assess the ability of *A. terricola* to feed upon the different bacterial isolates. A first procedure consisted in preparing bacterial lawns on buffered agar, inoculating the plate with a suspension of trophozoites (actively growing amoebae) and looking for clearing zones after about one week of incubation. The bacterial lawn was prepared by centrifuging aseptically a 2 day-old culture of a particular bacterial strain, washing it twice with the PYG medium in which the organic compounds, except for the citrate chelator, were omitted, resuspending the pellet in the organic-free PYG medium and spreading half of the suspension on an agar plate. The other half of the suspension was used in the second procedure. In this case, the bacterial suspension was further diluted with the organic-free PYG medium and inoculated with a drop of a trophozoite suspension that was concentrated by centrifugation. A decrease in the optical density of the suspension and an increase in protozoan numbers (measured in a hemacytometer cell with a light microscope) were indicative of the occurrence of predation. The first procedure showed that the four strains tested (B0649, B0483, B0577, and B0550) are being fed upon by *A. terricola*. After 10 to 14 days the bacterial lawns had disappeared. *Arthrobacter spp.* used in our previous experiments was also tested and turned out to be resistant to predation by *A. terricola*. The second procedure confirmed these results. The four strains were being fed upon at very different rates. For example, the suspension with the strain B0577 became almost clear after two weeks at which time the protozoan population had increased from a nondetectable

level (less than 200 cells per mL) to 4.6 105 cells per mL. On the other hand, the B0649 and B0550 suspension lost their turbidity only after four weeks at which time the protozoan population was estimated at 2.7.105 and 9.8.105 cells per mL, respectively. The B0483 strain was fed upon at an intermediate rate. These feeding rates are quite low. The presence of a capsule around the bacterial cells may explain why their populations are decimated so slowly by the amoebae.

Isolation of mutants unable to excrete polymers:

A possible way to assess accurately the role played by bacterial EPS secretions in reducing the saturated hydraulic conductivity of porous media is the use of non-EPS-producing mutants. Such mutants may also help to determine the influence of the bacterial capsule on the rate of protozoan grazing. In order to select spontaneous mutants not producing EPS, or producing them to a lesser extent, the isolates were grown in PTYG broth and kept in the exponential phase of growth for 8 days by regular transfer to fresh broth at 2 day intervals. The success of this method relies on the hypothesis that the cells that stop producing EPS can reproduce faster. The potential mutants were screened by looking for nonmucoid colonies on plates streaked with culture samples taken at various times. Both PTYG and defined media were used for screening. A nonmucoid mutant could be isolated from cultures of B0693 and B0550. The API Rapid NFT test was used to make sure that the nonmucoid variants arose from the parent strain and not from accidental contamination. API test results matched in the two cases with the parent strains. Microscopic examination showed that the nonmucoid variants are still encapsulated but that their capsule is much thinner.

Use of different carbon sources:

The carbon source used up to now in the percolation experiments, i.e., glucose, was convenient to study the fundamentals of bacterial clogging of porous

media but is an unlikely microbial substrate in bioremediation schemes. When the carbon source is the pollutant itself, it is by nature much more recalcitrant to microbial degradation than simple carbohydrates and when injected as a supplement to stimulate cometabolic processes, it is desirable that the carbon source be itself slightly recalcitrant to allow its transport to polluted zones situated at some distance from the injection well. We are currently screening different substrates for their kinetics of degradation by the strains B0550 and B0693 and their respective nonmucoid variants.

Preliminary results indicate that 2-phenylbutyric acid is not acted upon by these strains and that malic acid is degraded at a similar rate as glucose. Interestingly, when strain B0693 is grown on malate, EPS are not being produced.

Bacterial clogging via gas production

The major problem encountered so far in our experiments involving methanogens has been the slow growth of these organisms under room temperature, much slower than at 37C where they are usually grown. In the last few months, various attempts have been made to decrease the doubling time of the particular strain (*Methanosarcina barkeri*) that we have selected. The pH has been brought down to optimal levels by replacing the original carbonate buffer with a phosphate buffer. However, the ensuing reduction in bicarbonate concentration has lowered the major source of sodium, which seems to appreciably affect the growth of *Methanosarcina barkeri* when methanol is the limiting substrate. Recent results seem to indicate that, with sodium available at an adequate concentration, we are now able to make *Methanosarcina barkeri* grow sufficiently fast to make percolation experiments feasible. These experiments will be conducted in the next few months, using the setup described in earlier reports.

Two months ago, we started looking into the possibility of using denitrifiers instead of methanogens to study the effect of gas production on the

clogging of natural porous media. The advantage of denitrifiers is that they are a lot less fastidious to cultivate (i.e., require far less precautions) and have smaller double times than the methanogens. A possible disadvantage, however, is that the denitrifiers are metabolically much more efficient than the methanogens and, therefore, produce much more biomass per mole of gas released in the pore space. Therefore, in experiments with denitrifiers, it is much more likely that the observed clogging will be the compounded effect of gas entrapment and cell accumulation. If the goal is to elucidate mechanisms, therefore, methanogens would be more interesting to use. For practical purposes, however, both types of experiments are worth being conducted because they are an essential complement to the work in progress on strictly aerobic bacteria. Therefore, we intend to pursue work with the denitrifiers in parallel with that involving the methanogens.

6. REFERENCES

Bernofsky, C. and Swan, M. 1973. "An improved cycling assay for nicotinamide adenine dinucleotide." Analytical Biochemistry, 53, 452-458.

Boyles, J. 1984. "The use of primary amines to improve glutaraldehyde fixation." Science of Biological Specimen Preparation, 7-21. SEM Inc., AMF O'Hare (Chicago), IL 60666-0507.

Burlage, R.S., Hooper, S.W. and Sayler, G.S. 1989. "The TOL (pWWO) catabolic plasmid." Applied and Environmental Microbiology, 55:6, 1323-1328.

Friedel, R.A. and Orchin, M. 1951. Ultraviolet Spectra of Aromatic Compounds. John Wiley & Sons, Inc., New York.

Frind, E.O. 1982. "The principle direction technique: A new approach to groundwater contaminant transport modeling." Finite Elements in Water Resources, pp. 13-25 - 13-41. K.O. Holz et al., (eds.). Springer Verlag, Berlin.

Fritz, J.S. and Schenk, G.H. 1979. Quantitative Analytical Chemistry, 4th Ed. Allyn and Bacon, Inc., Boston.

Gillham, R.W. and Cherry, J.A. 1982. "Contaminant migration in saturated unconsolidated geologic deposits." Recent Trends in Hydrogeology. Geologic Society of America Special Paper 189. T.N. Narasimhan (ed.). The Geological Society of America, Boulder, CO.

Harrison, D.E.F., MacLennan, D.C. and Pirt, S.J. 1969. "Response of bacteria to dissolved oxygen tension." In Fermentation Advances, D. Perlman (ed.), Academic Press, London, pp. 117-144.

Heath, M.S., Wirtel, S.A. and Rittmann, B.E. 1990. "Simplified design of biofilm processes using normalized loading curves." Research Journal Water Pollution Control Federation (WPCF), 62:2, 185-192.

Klotz D. and Moser, H. 1974. "Hydrodynamic dispersion as aquifer characteristic model experiments with radioactive tracers." Isotope Techniques in Groundwater Hydrology, 2, 341-355. International Atomic Energy Agency, Vienna.

Koch, A.L. 1981. "Growth measurement." Manual of Methods for General Bacteriology, pp. 179-207, ed. by P. Gerhardt et al. Americal Society for Microbiology, Washington, DC.

Matin, A. and Gottschal, J.C. 1976. "Influence of dilution rate on NAD(P) and NAD(P)H concentrations and ratios in a Pseudomonas sp. grown in continuous culture." J. Gen. Microbiol., 94, 333-341.

McAuliffe, C. 1969. "Solubility in water of normal C_9 and C_{10} alkane hydrocarbons." Science, 163:3866, 478-479.

McLeod, F.A., Lappin-Scott, H.M. and Costerton, J.W. 1988. "Plugging of a model rock system by using starved bacteria." Appl. Env. Microb. 54, 1365-1372.

Miller, C.T., Poirier-McNeill, M.M. and Mayer, A.S. "Dissolution of trapped nonaqueous phase liquids: Mass transfer characteristics." Water Resources Research, in press.

Nicoud, R.M. and Schweich, D. 1989. "Solute transport in porous media with solid-liquid mass transfer limitations applications to ion exchange." Water Resources Research, 25:6, 1071-1082.

Rittmann, B.E. and P.L. McCarty. 1981. "Substrate Flux into Biofilms of Any Thickness." J. Environ. Eng., 107, 831-849.

Rosenberg, M., Gutnick, D. and Rosenberg, E. 1980. "Adherence of bacteria to hydrocarbons: A simple method for measuring cell surface hydrophobicity." FEMS Microbiology Letters, 9:1, 29-33.

Shames, I.H. 1982. Mechanics of Fluids, 2nd ed. McGraw-Hill Book Company, New York.

Suidan, M.T., Rittmann, B.E. and Traegner, U.K. 1987. "Criteria establishing biofilm-kinetic types." Water Research, 21:4, 491-498.

Vandevivere, P. and Baveye, P. 1990. "Saturated hydraulic conductivity reduction caused by strictly aerobic bacteria in sand columns." Submitted to Soil Science of America Journal.

Welty, J.R., Wicks, C.E. and Wilson, R.E. 1984. Fundamentals of Momentum, Heat, and Mass Transfer, 3rd edition. John Wiley & Sons, New York.

Wheeler, M.F. 1988. "Modeling of highly advective flow problems." In Developments in Water Science, Vol. 1. Modeling Surface and Sub-Surface Flows. Elsevier, pp. 35-44.

Wheeler, M.F. and Dawson, C.N. 1987. an Operator-Splitting Method for Advection-Diffusion-Reaction Problems. Department of Mathematical Sciences, Rice University, Technical Report 87-9.

Wilson, D.F., Erecinska, M., Drown, C. and Silver, I.A. 1977. "Effect of oxygen tension on cellular energetics." Am. J. Physiol., 233, C135-C140.

END

DATE FILMED

12/19/90